The Pennsylvania State University

The Graduate School

Department of Civil and Environmental Engineering

BACTERIAL ADHESION TO METAL OXIDE SURFACES IN THE PRESENCE OF NATURAL ORGANIC MATTER

A Thesis in

Environmental Engineering

by

Charles John Winslow III

Submitted in Partial Fulfillment
of the Requirements
for the Degree of

Master of Science

August 2009

The thesis of Charles John Winslow III was reviewed and approved* by:

Bruce E. Logan
Kappe Professor of Environmental Engineering
Thesis Advisor

William D. Burgos
Professor of Environmental Engineering
Professor in Charge of Graduate Programs

James D. Kubicki
Associate Professor of Geochemistry

*Signatures are on file in the Graduate School

ABSTRACT

An understanding of the interaction between natural organic matter and metal oxides is critical to predicting bacterial adhesion in natural systems. The objective of this research was to examine bacterial adhesion to various metal oxide surfaces in the presence of humic acids using nanoscale atomic force microscopy (AFM) experiments. AFM was used to measure the adhesion force between standard silicon nitride AFM probes (i.e. bacterial surrogates) and various surfaces before and after humic acid adsorption as a function of residence time. Five surfaces were analyzed in this study, including three metal oxide surfaces (Fe_2O_3, Al_2O_3, and TiO_2), a glass microscope slide (SiO_2), and freshly-cleaved muscovite mica. Adhesion to each surface was quantified in terms of both the *overall* interaction between the AFM probe and the surface (i.e. the average force or F_{avg}) as well as the *localized* interaction between the AFM probe and the stickiest five percent of the surface sites (i.e. the sticky force or F_5). Spectral force analysis (SFA) was introduced as a useful tool for analyzing the distribution of adhesion forces on a surface by simultaneously providing insight into the effect of humic acid adsorption, residence time, and the small number of highly sticky surface sites.

Adhesion force to the uncoated surfaces increased in the order SiO_2 < mica < TiO_2 < Al_2O_3 < Fe_2O_3, irrespective of whether the average (F_{avg}) or sticky (F_5) forces were analyzed. Increasing the tip-surface residence time resulted in an overall increase in adhesion force but not a change in the relative stickiness of the five surfaces. At short residence times (i.e. zero seconds) humic acid adsorption resulted in an increase in adhesion force on all surfaces except mica and Fe_2O_3, irrespective of whether the average forces or sticky forces were analyzed. At long residence times (i.e. ten seconds) humic

acid adsorption resulted in an increase in adhesion force on all surfaces except mica and Fe_2O_3 when considering the average forces. When considering the sticky forces at long residence times, humic acid adsorption resulted in an increase in adhesion force on all surfaces except Fe_2O_3.

No consistent explanation could account for the observed results, although arguments based on electrostatics and surface roughness could explain the tip-surface interaction in certain instances. It was concluded that standard silicon nitride AFM probes are not ideal bacterial surrogates, so further work with colloid AFM and bacteria is needed to better understand bacterial adhesion to metal oxides in the presence of natural organic matter.

TABLE OF CONTENTS

LIST OF FIGURES

LIST OF TABLES

ACKNOWLEDGEMENTS

Many thanks to my advisor, Dr. Bruce Logan, for offering me the opportunity to work in his laboratory, assisting me with my AFM research, and patiently sticking with me until the very end. Thanks also to Dr. William Burgos and Dr. James Kubicki for their insightful comments along the way. I am indebted to Dr. Lichong Xu for the countless hours he spent teaching me to use the atomic force microscope. Most important of all, not to be forgotten is Victoria, my loving and supportive wife, whose patience and encouraging words provide the inspiration and foundation for all my accomplishments.

This research was supported by the National Science Foundation under Grant No. CHE-0431328.

1 INTRODUCTION

The ubiquitous nature of bioadhesion and subsequent biofilm formation provides motivation for obtaining a better understanding of how bacteria adhere to and colonize natural and manufactured materials. The vast amount of research on bacterial adhesion has focused on a number of natural systems (Walker, 2005; Ryan et al., 1999) and engineered processes (Bentham, 1993; Walker et al., 1991; Baier, 1982).

The objective of the research reported here was to examine bioadhesion to various metal oxide surfaces in the presence of humic acids using nanoscale AFM experiments, such as might occur in a groundwater aquifer. The central hypothesis of this research was that bacterial adhesion to surfaces depends primarily on the number and distribution of "sticky" surface sites resulting from the intrinsic heterogeneity of all surfaces. Therefore, the adhesion of molecules and bacteria to surfaces first occurs at the stickiest sites (fast kinetics) followed by the less sticky sites (slow kinetics). Extending this work to organic polymers, it was proposed that humic acid adsorption to metal oxide surfaces would preferentially occur at surface sites in order of decreasing stickiness, and that the net effect of this adsorption would produce a modified surface less favorable to initial bacterial adhesion. However, it was further hypothesized that long residence times between bacteria and humic-coated metal oxide surfaces could negate this effect as a result of conformational changes of the polymer as well as the establishment of chemical bonds between organic functional groups and the bacterial surface.

Laboratory work consisted of measuring the adhesion force between standard silicon nitride AFM probes and various surfaces. Freshly cleaved mica served as a control surface while vapor deposited iron, aluminum, and titanium oxides and glass microscope

slides rounded out the suite of surfaces studied. Adhesion force measurements were conducted in a solution of ultrapure water both before and after humic acid adsorption. By measuring these forces over time, the effect of residence time on the magnitude of the adhesion force was determined to obtain a more accurate model of molecular scale interactions. AFM topographical images provided surface characterization of the uncoated and humic acid-coated surfaces.

From previous work and chemical arguments, one might expect the adhesion force to increase in the order $SiO_2 < TiO_2 < Al_2O_3 < Fe_2O_3$ on the uncoated surfaces (Vadillo-Rodriquez and Logan, 2006; Li and Logan, 2004), with the humic acid coating decreasing the magnitude of the measured force. Increasing the tip-sample residence time should generally increase the adhesion force because it allows for conformational changes of the polymer and the establishment of chemical bonds (Xu et al., 2005). Thus, another objective of this research was to demonstrate that in the presence of humic acids, the adhesion force at long residence times will exceed that of the uncoated surface at the same residence time.

2 LITERATURE REVIEW

2.1 Bacterial Adhesion Overview

Bacterial adhesion and subsequent biofilm formation impact a variety of natural and engineered systems. Bacterial adhesion has been examined relative to environments such as the human body (Montanaro et al., 2004; Méndez-Vilas et al., 2004), water treatment facilities (Namguk et al., 2007; Hilal, Mohammad et al., 2003; Hilal, Al-Khatib et al., 2003), water distribution systems (Gamby et al., 2008; Walker et al., 1991; Maronek, 1988), heat exchangers (Bentham, 1993; Tobin et al., 1981;), marine surfaces (Clint, 2001; Jagels et al., 1995; Dempsey, 1981), and in situ bioremediation sites (Bell et al., 2005; Sanin, 2004; Li and Logan, 1999).

Understanding and predicting bacterial adhesion, whether in natural or engineered systems, is a difficult task because of the complex factors affecting adhesion between a bacterium and a surface. Researchers have studied bacterial adhesion in terms of surface hydrophobicity (Salerno et al., 2004; Bruinsma et al., 2001), surface charge (Stefano et al., 2000; Gottenbos et al., 1999), surface roughness (Tang et al., 2006; Shellenberger and Logan, 2002), and solution chemistry (Gexin and Walker, 2007; Camesano and Logan, 1998), among other factors.

2.2 Bacterial-Surface Interactions: Theory versus Experiment

Theoretical predictions of bacterial-surface interactions do not always prove accurate when tested in the laboratory. For instance, contrary to thermodynamic predictions, bacterial adhesion has been observed in cases where the hydrophobicity of

the cell surface would have suggested relatively low adhesion (Millsap et al., 1996; Absolom et al., 1983). In many other studies bacterial adhesion has been observed even when theoretical predictions suggest a repulsive electrostatic potential energy barrier between the bacterium and surface (Smets et al., 1999; Rijnaarts et al., 1999; Truesdail et al., 1998).

One explanation of this inconsistency between theory and experiment focuses on the inherent heterogeneity of surfaces (Whitehead et al., 2006). Recent atomic force microscopy (AFM) research highlighted the importance of surface heterogeneity in correlating the adhesion response between an AFM tip and various metal oxide surfaces to macro scale bacterial adhesion experiments using these same surfaces (Vadillo-Rodriguez and Logan, 2006). This work provided evidence that surface heterogeneity produces localized, highly favorable sites for bacterial attachment that control the overall adhesion response of a surface.

2.3 Bacterial Adhesion to Metal Oxides

Metal oxide surfaces have a great effect on bacterial adhesion in natural environments. Iron oxides, in particular, are known to increase bacterial adhesion, which has been extensively documented in the literature (Parikh and Chorover, 2006; Li and Logan, 2004; Ryan et al., 1999; Johnson and Logan, 1996). Consider an idealized system consisting of a quartz particle and a single bacterium. Under most environmental conditions there exists an electrostatic repulsion between the two surfaces because bacteria and quartz particles typically possess a negative charge in solutions typical of groundwater systems. However, the adsorption of metal oxide onto quartz gives the

surface a positive charge, thus increasing bacterial deposition on the surface. In reality the inherent complexity of natural systems makes such an idealized view too simplistic. For example, in environmental systems one needs to account for the presence of natural organic matter (NOM) and other chemicals.

2.4 Bacterial Adhesion in the Presence of Natural Organic Matter

Humic substances play an integral role in environmental systems. Their function as a major constituent of total dissolved organic matter as well as their buffering capacity proves important to a large variety of geochemical reactions, but of even greater interest pertaining to this research concerns their interactions with other compounds and elements in the environment. NOM has a significant influence on bacterial adhesion in the idealized system discussed above. When negatively charged organic matter adsorbs to a metal oxide surface, one can reasonably expect a decrease in bacterial adhesion to the surface because the natural organic matter shields the positive charge of the underlying metal oxide (Park and Kim, 2009; Johnson and Logan, 1996).

2.5 Atomic Force Microscopy (AFM)

2.5.1 History of AFM

Binnig et al. (1986) developed the atomic force microscope (AFM), the last in the series of scanning probe microscopes invented in the 1980s, by combining the principles of the scanning tunnel microscope (STM) and the stylus profilometer. Scanning tunnel microscopy, invented by Binnig and Rohrer in the early 1980s, allows for imaging of

conducting and semi-conducting surfaces using a tunneling current (Binnig and Rohrer, 1983). The stylus profilometer, first invented by Gustav Schmalz in 1929 and improved by Russell Young in 1971, allows for topographical imaging of surfaces (conducting and insulating) by raster scanning a sharp tip over the surface (Young, 1972; Schmalz, 1929). The atomic force microscope has proved more flexible than the scanning tunnel microscope because it can image not only conductors but also insulators, and it is an improvement on the stylus profilometer because it provides higher image resolution and causes less sample destruction.

An AFM is not only capable of imaging soft, insulating surfaces with minimal sample damage, but also of measuring forces between the sample surface and AFM probe at the molecular level. The AFM can create three-dimensional images of surfaces as tiny as an individual atom as well as measure forces as small as attonewtons (10^{-18} Newtons) (Binnig et al., 1986). The capabilities of AFM as a tool for both surface imaging (Jalili and Karthik, 2004; Maurice, 1996) and force measurement (Butt et al., 2005) have been well documented. AFM continues to be an important research tool in fields such as environmental geochemistry, biological sciences, biomaterials surface science, and nanotechnology, to name a few.

2.5.2 Operation of AFM

The basic components of an atomic force microscope consist of a laser light, lens, piezoelectric scanner, photodetector, and probe (consisting of tip, cantilever, and base) (Figure 2.1). AFM generally operates by quantifying the interaction of an AFM probe with a sample surface. The sample is securely mounted on the piezoelectric scanner. The

AFM probe consists of a sharp tip mounted on a flexible cantilever (both typically constructed of a reflective, metallic material such as silicon or silicon nitride), which in turn is mounted on a rigid base. A lens is used to direct the laser light on the cantilever, and the reflected light is absorbed by the photodetector. As the AFM tip interacts with a sample, the cantilever deflection is indirectly measured by changes in the location of the reflected laser light on the photodetector.

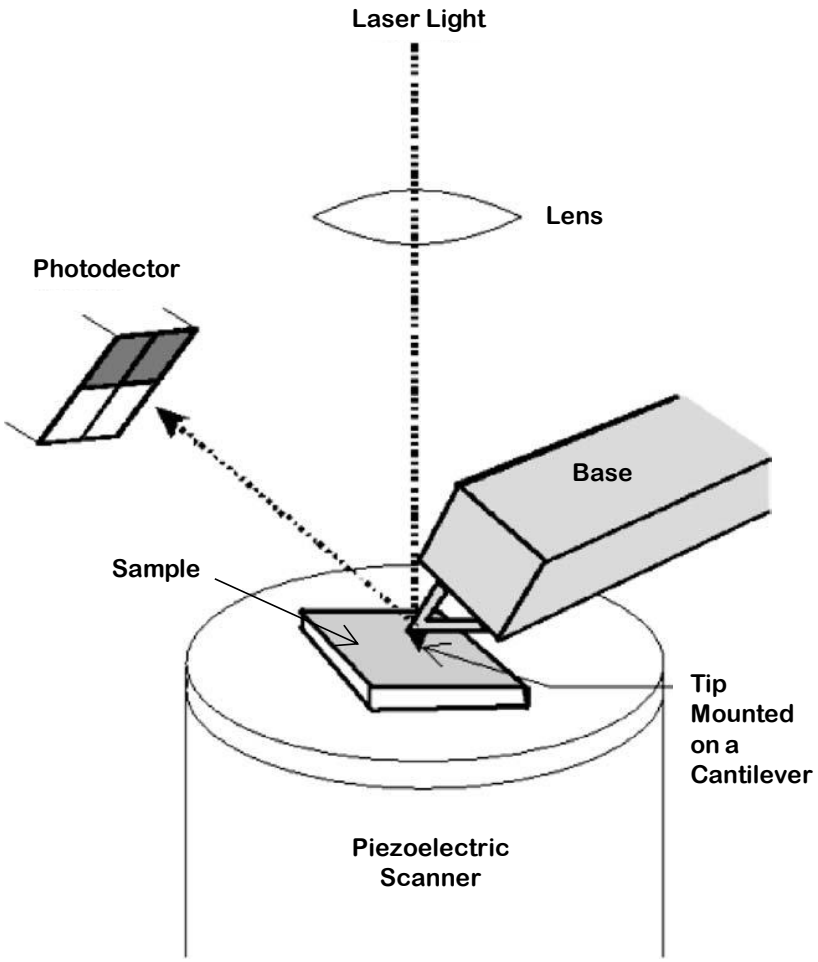

Figure 2.1: Schematic of an Atomic Force Microscope (AFM).
Adapted from H.-J. Butt et al. (2005)

2.5.3 Imaging with AFM

The two most common modes used for AFM imaging are contact mode and tapping mode. In both modes the sample surface is raster scanned beneath the stationary tip, although the tip-surface interaction is different in each instance. Depending on the make and model of the AFM, the tip may alternatively be raster scanned above the stationary sample surface, but this difference does not affect the quality of the image obtained. For the sake of clarity and consistency, all future references herein will assume the sample is scanned beneath the stationary tip, which is the operational mechanism employed by the AFM used in this research.

In the case of contact mode, the sample surface maintains constant contact with the tip as the scan progresses in the horizontal plane. The user-defined baseline deflection of the cantilever serves as the established setpoint, the magnitude of which depends on the surface under consideration. Surface features encountered during scanning deflect the cantilever, which changes the position of the reflected laser light on the photodetector. A feedback loop monitors changes in the tip deflection, and the piezoelectric scanner makes appropriate adjustments in the vertical direction to revert the tip deflection to the setpoint value.

In tapping mode the AFM cantilever vibrates above the sample and only makes intermittent contact with the surface. Tapping mode differs from contact mode in that the feedback loop maintains the cantilever at a constant amplitude instead of a constant deflection. Surface features encountered during scanning either dampen (in the case of protrusions) or increase (in the case of surface depressions) the amplitude of the cantilever vibration. The feedback loop monitors changes in the amplitude of the

cantilever, and the scanner adjusts the vertical position of the sample surface in order to return the amplitude to the setpoint value.

The choice of using contact mode or tapping mode depends primarily on the sample type. Contact mode is better suited for novice AFM users imaging hard surfaces. It is difficult to image soft samples using contact mode because the constant and forceful interaction of the tip and surface has the tendency to destroy the sample. Tapping mode can effectively image both hard and soft samples, but it is especially useful at imaging soft samples such as biological material that would otherwise be destroyed using contact mode (Dufrêne, 2002).

2.5.4 Force Measurements with AFM

AFM is a useful tool for measuring the adhesion force between a sample surface and an AFM probe. Measuring adhesion forces with an AFM involves moving the sample surface towards the AFM probe, deflecting the cantilever with the sample surface, and then retracting the sample surface to its original position before repeating the process again.

One can visualize the interaction between the probe and sample using a force curve, which shows the deflection of the cantilever (Z_c) versus the position of the piezo (i.e. scanner) (Z_p) (Figure 2.2). The far right of the figure depicts the initial position of the cantilever and sample where the distance between them is sufficient such that there is no interaction between them. Following the arrows to the left, the sample and probe begin to interact. Depending on the material characteristics of the sample and AFM tip, the interaction between the two may be either repulsive (as depicted in Figure 2.2) or

attractive (cantilever bent towards sample). Moving farther to the left, at some point the sample surface contacts the cantilever, deflecting it until a user-defined contact force is reached. Selection of the contact force, often referred to as the trigger threshold, should be sufficiently large such that it exceeds the initial attractive/repulsive force between the cantilever and sample. Once the trigger threshold is reached, the sample and probe maintain contact for a user-defined length of time (i.e. contact time). Once the contact time is reached, the sample begins moving away from the probe following the same path as the approach. Following the path down to the right, the sample continues to retract with the cantilever adhered to it. The cantilever remains adhered to the sample until the spring force of the deflected cantilever equals the adhesion force between the tip and surface, at which point the cantilever snaps off the surface and returns to its original non-contact position.

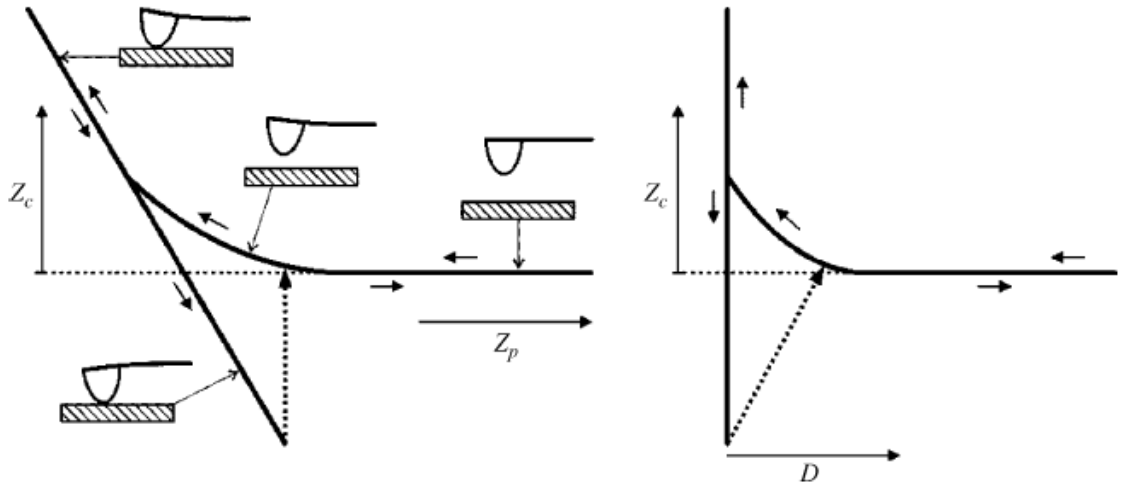

Figure 2.2: Schematic of a typical cantilever deflection-vs.-piezo height (Z_c-vs.-Z_p) curve (left) and corresponding Z_c-vs.-D plot, with $D = Z_c + Z_p$. Adapted from H.-J. Butt et al. (2005).

Calculation of the adhesion force between the AFM tip and the sample surface is based on the assumption that the AFM tip remains adhered to the sample surface until the adhesion force between the tip and sample equals the spring force of the deflected cantilever. Additionally, it is necessary to assume that the AFM cantilever is linear-elastic and behaves according to Hooke's Law, which states that the force exerted by a linear-elastic material is in direct proportion to the distance the material is deflected (either stretched or compressed) away from its equilibrium position, multiplied by the force constant (or spring constant) of the material.

Hooke's Law can be expressed mathematically as $F = -k \cdot Z_c$, where "F" is the adhesion force between the AFM tip and sample surface, "k" is the spring constant of the AFM cantilever, and "Z_c" is the deflection of the AFM cantilever from its equilibrium position. The deflection of the AFM cantilever can be extracted from the force curve. Methods for determining the cantilever spring constant have been well documented (Sader et al., 1995; Senden and Ducker, 1994; Cleveland et al., 1993), but the most widely accepted and adopted method in use today is the thermal tune method (Serry, 2005; Hutter and Bechhoefer, 1993). Once the cantilever spring constant and cantilever deflection are known, calculation of the adhesion force is a simple matter of multiplication.

3 MATERIALS AND METHODS

3.1 Adsorption Experiments

3.1.1 Surface Preparation

Five surfaces were analyzed in this study. Three metal oxide surfaces included vapor-deposited iron oxide (Fe_2O_3), aluminum oxide (Al_2O_3), and titanium oxide (TiO_2) (all materials custom manufactured by PPG Industries). Micro cover glass (SiO_2) (VWR International) was chosen as a fourth surface, and freshly-cleaved muscovite mica (Electron Microscopy Sciences) was used as a control surface. All surfaces were secured to AFM sample pucks (Veeco Probes) with 60-minute epoxy (Loctite), which was allowed to fully cure for at least 24 hours before cleaning the surfaces.

The metal oxide and glass surfaces were cleaned in a solution consisting of 3 mL DART 210 glass cleaning solution (Madison Chemical) in 1500 mL ultrapure water. The solution was heated to 60°C while continuously stirred, and then the surfaces were sonicated in the heated solution for 20 minutes. After a thorough rinsing with ultrapure water, the surfaces were sonicated for 10 minutes in ultrapure water preheated to 45°C. A final rinsing with copious amounts of ultrapure water followed by drying with nitrogen gas completed the cleaning process.

Muscovite mica surfaces were not chemically cleaned but were freshly-cleaved before use.

All uncoated surfaces were analyzed immediately after the cleaning process, and were subsequently stored at 4°C in sterile, airtight Petri dishes (Pall Corporation). Surfaces were warmed to room temperature prior to further analysis.

3.1.2 Humic Acid Preparation

Elliott soil humic acid standard (International Humic Substances Society) was adsorbed to all surfaces. A 500 mL solution of 100 mg/L humic acid was prepared and subsequently titrated to pH 4.5 (±0.1). The humic acid solution was gently mixed overnight at room temperature using a magnetic stirrer to reach equilibrium, and the pH was again adjusted to 4.5 (±0.1). The solution was stored at 4°C prior to use, at which time it was warmed to room temperature and adjusted to pH 4.5 (±0.1) if necessary. Fresh humic acid solution was prepared at least every three months.

3.1.3 Adsorption Procedure

Cleaned (or cleaved, in the case of muscovite mica) surfaces were each placed in individual sterile, airtight Petri dishes (Pall Corporation) that were then completely filled with humic acid solution. The Petri dishes were sealed and gently shaken overnight (16-18 hours) on a table shaker at 150 revolutions per minute. Each surface was gently rinsed with ultrapure water so as to remove any reversibly adsorbed humic material. Rinsed surfaces were then transferred to new partially-sealed Petri dishes that were subsequently placed in a desiccator overnight (22-24 hours).

All humic acid-coated surfaces were analyzed immediately after the drying process, and were subsequently stored at 4°C in sterile, airtight Petri dishes (Pall Corporation). Surfaces were warmed to room temperature prior to further analysis.

3.2 AFM Experiments

3.2.1 Instrumentation and Software

Atomic force microscopy experiments were performed with a MultiMode AFM attached to a Nanoscope IIIa scanning probe microscope controller and PicoForce force spectroscopy control module (Digital Instruments). An optical viewing system consisting of a bracing apparatus (Olympus, model SZ-STS) and an optical microscope (Nikon) provided an overhead view of the probe and sample, with the output displayed on a color monitor (Sony). The computer connected to the AFM utilized version 6.12r2 software (Digital Instruments) to analyze the raw data. The microscope sat atop an XY transition stage and silicone vibration pad (Newport, model 401), which in turn rested on an integrated vibration isolation table (Technical Manufacturing Corporation). The controllers and computer equipment were positioned on an adjacent laboratory table.

3.2.2 Force Microscopy Setup and Procedure

All force microscopy experiments were done in fluid using contact mode. Standard silicon nitride probes (model DNP) were used with a nominal cantilever spring constant of 0.12 N/m. Probes were UV treated for 30 to 45 minutes immediately before use in order to remove molecular organic contamination. Cleaned and prepared surfaces

(uncoated or humic acid-coated) were magnetically secured on the PicoForce scanner. AFM probes were positioned in the fluid cell probe holder (Veeco Probes, model MTFML), which was then secured within the low noise optical head (model LN). The optical head was then placed atop the scanner and held in place with the supplied springs.

The background fluid for all experiments consisted of ultrapure water, which was added to the fluid cell probe holder after securing the optical head to the scanner and obtaining a watertight seal between the fluid cell O-ring and the sample surface. The process involved transferring fresh ultrapure water to a sterile, 10 mL syringe (BD, model 301604), which was then used to pump the fluid through a 0.22 μm pore size nylon syringe filter (Restek, model 26148) and into the fluid cell probe holder via nonreactive plastic fittings and rubber tubing (Veeco Probes). The filter was flushed with 10 mL of ultrapure water before use to remove any residue or contaminants remaining from the manufacturing process.

Special attention was exercised to avoid the formation of air bubbles while injecting ultrapure water into the fluid cell probe holder. Before fluid injection the sample was manually raised until it made contact with the fluid cell O-ring. After fluid injection the fluid cell probe holder input and output lines were clamped to prevent fluid escape, and the optical viewing system was utilized to ensure no air bubbles developed on or near the cantilever. If any air bubbles were visible, the plastic tubing clamps were undone, and small bursts of fluid were pushed through the fluid cell to displace the bubbles.

Once the fluid cell probe holder was filled with ultrapure water and it was determined that no air bubbles were present, the AFM laser was connected. The laser was aligned on the end of the probe cantilever using a combination of the optical viewing

microscope method and the projection method to ensure accuracy (Veeco Instruments, 2004). After laser alignment the SUM voltage signal was maximized by first adjusting the photodetector mirror and then the X- and Y-axis photodiode positioners. Most probes displayed SUM signals between 5.5 and 6.0 volts, and no probe with a SUM signal less than 5.0 volts was used in any experiment.

Following the laser alignment the sample was automatically engaged with the cantilever tip. Immediately after engagement the deflection sensitivity of the cantilever was determined in force calibration mode. The surface was withdrawn from the tip at least 125 nm, and the spring constant of the cantilever was measured using the thermal tuning method. If the calculated cantilever spring constant deviated more than 10 percent from the nominal value of 0.12 N/m, the probe was discarded. After checking the spring constant, the surface and probe were again automatically engaged.

All force measurements were done in relative trigger mode with a trigger threshold of 3 nN and surface residence times of zero, one, and ten seconds. For each force measurement, these settings resulted in the sample surface pushing into and bending the cantilever until it deflected the equivalent of 3 nN. For instance, a cantilever with a spring constant of 0.12 N/m would experience a 3 nN force after deflecting 25 nm (i.e. 3 nN ÷ 0.12 N/m = 25 nm). After reaching this 3 nN trigger threshold, the sample surface remained in contact with the cantilever for the duration of the residence time before retracting from the cantilever.

Three random surface sites were examined for each sample surface. The adhesion forces between sample surface and cantilever tip were measured over a 10 μm by 10 μm

scan area with 1 μm interval spacing. Therefore, 100 forces were measured at each of the three surface sites, yielding 300 force measurements per sample surface.

3.2.3 Topographical Imaging Setup and Procedure

All topographical imaging experiments were done in air using tapping mode. Standard silicon probes (model RTESP) with a nominal resonant frequency of 300 kHz were used for all experiments. In order to remove molecular organic contamination, probes were UV treated for 30 to 45 minutes immediately before use. Cleaned and prepared surfaces (uncoated or humic acid-coated) were magnetically secured on the PicoForce scanner. AFM probes were positioned in the air probe holder (Veeco Probes, model MMEFCH), which was then secured within the low noise optical head (model LN). The optical head was then placed atop the scanner and held in place with the supplied springs.

As in contact mode, the laser was aligned on the probe tip using a combination of the optical viewing microscope method and the projection method to ensure accuracy (Veeco Instruments, 2004). The mirror and photodetector were adjusted to maximize the root mean square laser signal amplitude and the SUM voltage. Typical RMS and SUM values for RTESP probes were 0.25 volts and 1.75 volts, respectively. Probes with an RMS signal less than 0.20 volts or a SUM signal less than 1.5 volts were discarded. The vertical voltage difference was also zeroed, indicating the laser beam was well centered on the probe tip.

After the laser and photodetector were adjusted, the resonance peak of the cantilever was determined automatically using the auto tune feature. The drive amplitude

was set and the operating point defined, and the sample surface was automatically engaged with the cantilever probe. After engagement the gain settings were optimized by first increasing the proportional gain until the piezo began to oscillate. The integral gain was set at two times the proportional gain, while the look ahead gain was set to zero. The setpoint was then minimized in order to reduce the force applied to sample surface via the probe tip.

At least three surface sites were imaged on each of the 15 sample surfaces. All sites were imaged over both a one and five micron scan area using a one hertz scan rate.

3.3 AFM Data Analysis

3.3.1 Adhesion Force Analysis

AFM raw force data was exported as ASCII code into Origin graphing and data analysis software (OriginLab, version 7.5), and then copied into Excel (Microsoft) for final analysis. Each individual force measurement produced a unique force curve that was stored as a separate raw data file. A total of 300 files were exported for each sample surface (100 force measurements per surface site, and three surface sites per sample).

Raw force data requires manipulation in order to yield a force because it is actually a record of cantilever deflection as a function of scanner head (i.e. surface) movement, both in units of nanometers. In order to convert the raw data into adhesion force measurements, the cantilever deflection was first determined from the retraction raw force curves (i.e. when the sample surface is retracted from the probe tip). This can

be visually interpreted as the vertical distance between the undeflected cantilever and the point of greatest deflection.

For each sample two statistical computations were done on the calculated forces. The "average" force was defined as the arithmetic mean of the combined 300 force measurements from the three separate surface sites. The "sticky" force was defined as the arithmetic mean of the highest 5% of the forces from the same 300 force measurements. In other words, when the 300 forces were ordered from highest to lowest, the "sticky" force was computed by averaging the 15 highest forces.

Cumulative force distribution curves were produced from the individual adhesion force data by ordering the individual forces from highest to lowest and plotting the cumulative sum of the forces as a function of the last individual adhesion force added to the cumulative sum (Ma et al., 2008). Each point on the cumulative force distribution curve corresponded to the sum of all the adhesion forces greater than or equal to the adhesion force at that point. Each curve was produced from 300 adhesion forces (100 forces from each of three surface sites). Utilizing this approach allowed for visualization and extraction of the average (F_{avg}) and sticky (F_5) adhesion forces, as well as the spectral force distribution over the scanned areas.

Uniformity of the reported adhesion forces was quantified by calculating the standard deviation of the forces on each sample surface both before and after humic adsorption. Weibull functions were fit to each skewed data set (i.e. 300 forces) using Excel (Microsoft), with the Weibull shape and scale parameters computed using Weibull++ (ReliaSoft, version 7.5.8). The standard deviations of the Weibull data sets were then calculated using Excel.

3.3.2 Topographical Image Analysis

All images were flattened via a zero order polynomial in order to improve clarity and remove minor noise distortions. For each surface a representative image was selected from among those available. Surface roughness was tabulated for the selected images. No additional editing was performed on any images, which were then saved as bitmap files. The bitmap format allowed for easier manipulation and arrangement of the images into a final product for presentation.

4 RESULTS

4.1 Adhesion Force Results

4.1.1 Relative Stickiness of Uncoated Sample Surfaces

The adhesion force between silicon nitride AFM tips and the five uncoated sample surfaces increased in the order SiO_2 < mica < TiO_2 < Al_2O_3 < Fe_2O_3 (Figures 4.1a and 4.1b). This result served as a baseline trend for comparison to the subsequent experiments examining the effect of humic acid adsorption on adhesion.

The range of forces considered did not affect the baseline trend. For instance, the same trend was observed whether the "average" or "sticky" forces were considered. However, the "average" force spectra produced a more distinct trend than that of the "sticky" forces.

4.1.2 Effect of Residence Time on Adhesion

Adhesion force correlated positively with tip-surface residence time when considering both the "average" (Figure 4.1a) and "sticky" (Figure 4.1b) adhesion forces. Adhesion force between silicon nitride AFM tips and the five uncoated sample surfaces was measured as a function of residence time in order to determine suitable residence times for later experiments. Residence times of zero, one, and ten seconds were originally considered. Longer residence times increased the tip-sample adhesion force. In all cases the magnitude of the increase in adhesion force between a zero second residence time and

a one second residence time was greater than that between a one second residence time and a ten second residence time.

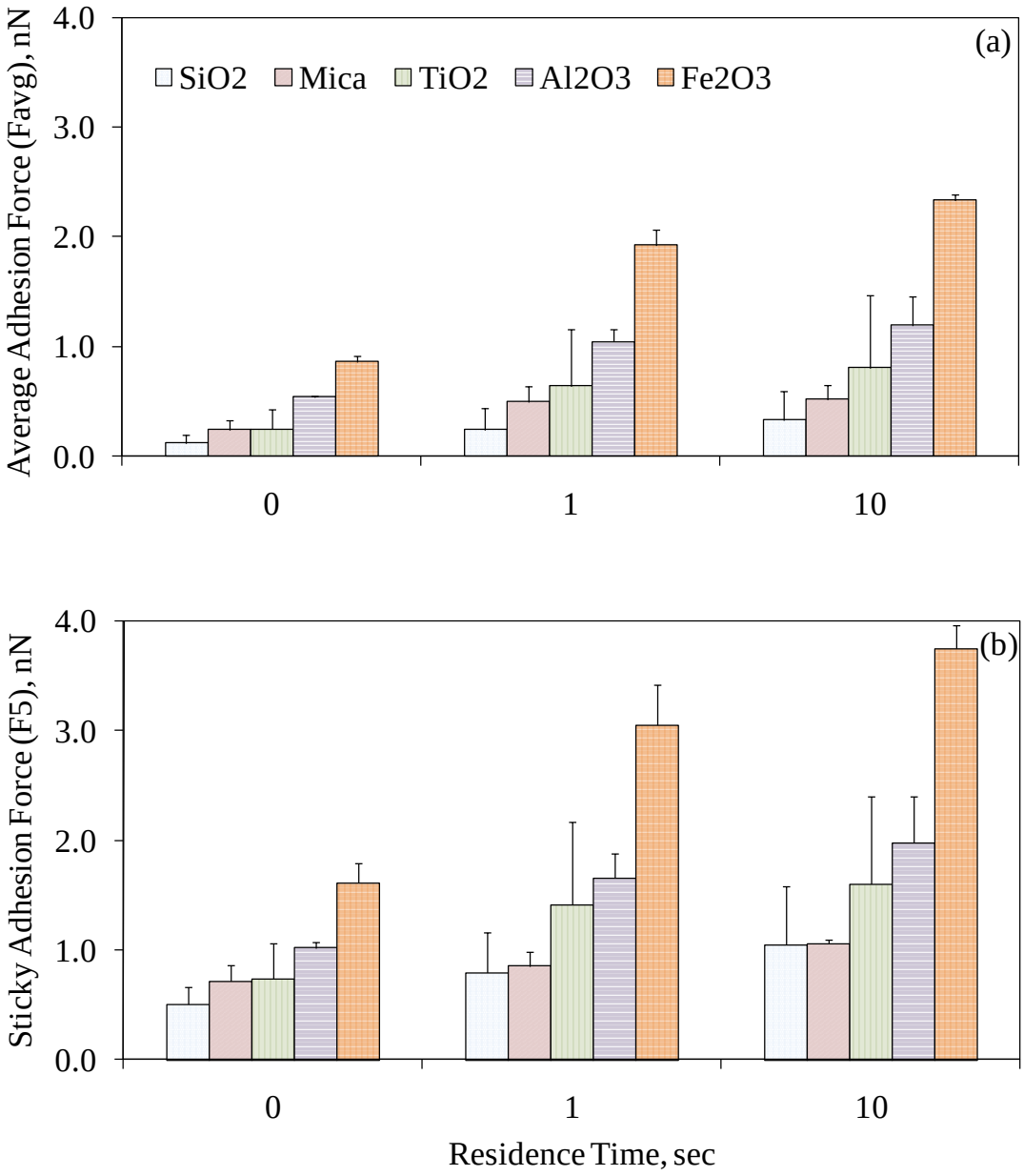

Figure 4.1: (a) Average and (b) Sticky adhesion forces on uncoated surfaces as a function of residence time.

Although no consistent trend could be identified between the standard deviation of the tip-surface adhesion force and sample surface, in general, the standard deviation of

the measured adhesion force increased with tip-surface residence time. This observation was noted in consideration of both the "average" and "sticky" forces. Furthermore, of the five uncoated surfaces, TiO_2 clearly exhibited the largest standard deviation.

To differentiate between adhesion forces resulting from "short" and "long" tip-surface residence times, the definitions of "short" and "long" residence times were established as zero and ten seconds, respectively, for all subsequent experiments. The shortest possible residence time consists of the scenario where the surface contacts the tip and immediately withdraws as soon as the three nN trigger threshold is reached (i.e. a zero second residence time). Although no upper limit to residence time theoretically exists, the AFM exhibited instability at residence times greater than ten seconds (data not shown).

4.1.3 Effect of Humic Acid Adsorption on Adhesion

At short (i.e. zero second) residence times, humic acid adsorption increased the average (F_{avg}) adhesion force on all surfaces except mica and Fe_2O_3 (Figure 4.2a). Humic acid adsorption resulted in the greatest increase in adhesion force on the SiO_2 surface, followed by the TiO_2 and Al_2O_3 surfaces, respectively. The adhesion force between silicon nitride AFM tips and the five humic coated sample surfaces increased in the order mica < Fe_2O_3 < TiO_2 ≈ Al_2O_3 < SiO_2. With the exception of mica, the presence of humic material increased the standard deviation of the measured adhesion force. The standard deviation of the coated surfaces increased in the order mica < Al_2O_3 < Fe_2O_3 < TiO_2 < SiO_2. With the exception of TiO_2 and Al_2O_3, the standard deviations of the uncoated surfaces were roughly the same.

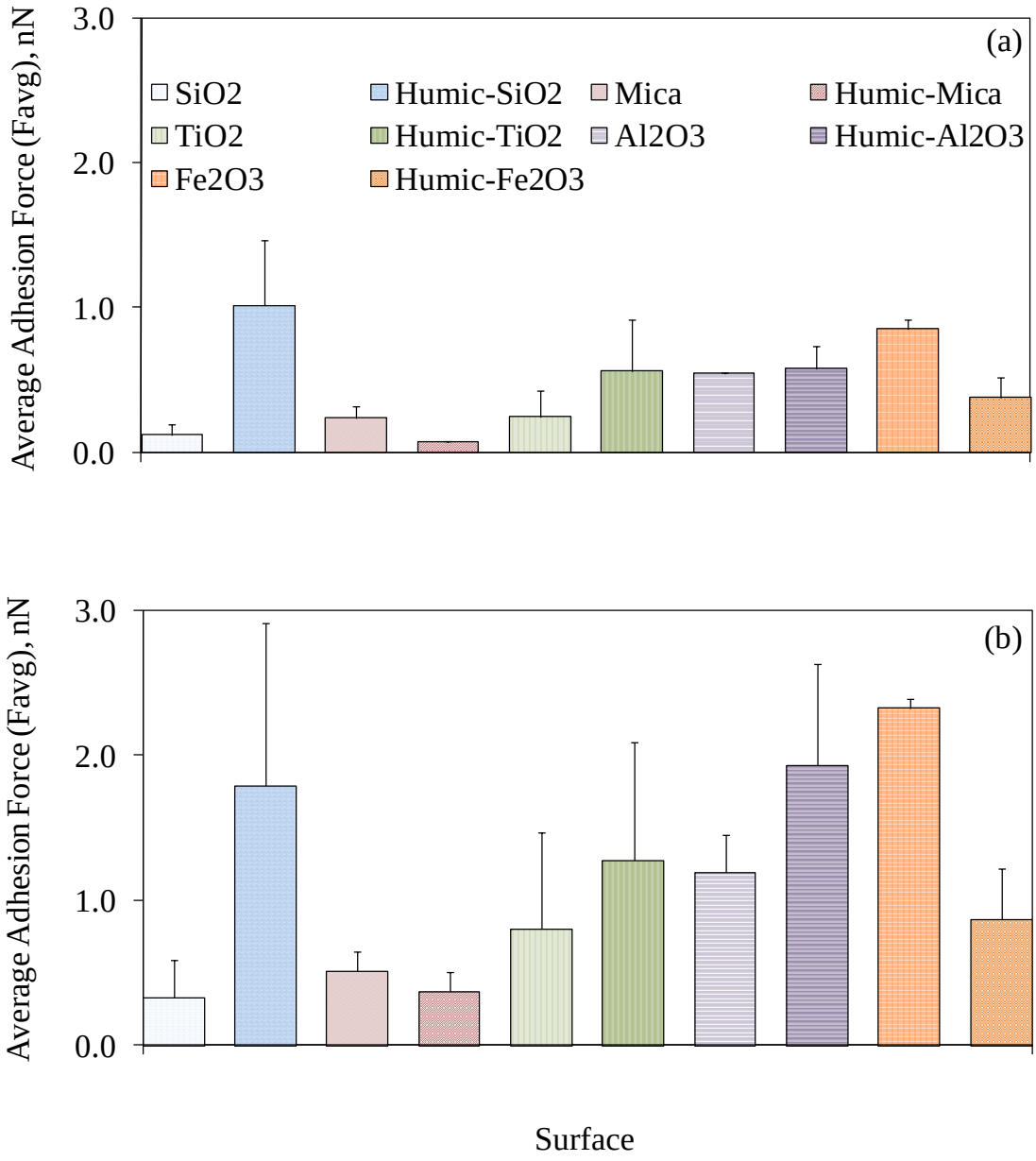

Figure 4.2: Average adhesion forces (F_{avg}) on uncoated and humic acid-coated surfaces at (a) short (zero seconds) and (b) long (10 seconds) residence times.

At long (i.e. ten second) residence times, humic acid adsorption increased the average (F_{avg}) adhesion force on all surfaces except mica and Fe_2O_3 (Figure 4.2b). Humic acid adsorption resulted in the greatest increase in adhesion force on the SiO_2 surface,

followed by the Al_2O_3 and TiO_2 surfaces, respectively. The adhesion force between silicon nitride AFM tips and the five humic coated sample surfaces increased in the order mica < Fe_2O_3 < TiO_2 < SiO_2 < Al_2O_3. On all surfaces the presence of humic material increased the standard deviation of the measured adhesion force. The standard deviation of the coated surfaces increased in the order mica < Fe_2O_3 < TiO_2 ≈ SiO_2 < Al_2O_3. The standard deviations of the uncoated surfaces increased in the order mica < Fe_2O_3 < TiO_2 < Al_2O_3 < SiO_2.

At short residence times, humic acid adsorption increased the sticky (F_5) adhesion force on all surfaces except mica and Fe_2O_3 (Figure 4.3a). Humic acid adsorption resulted in the greatest increase in adhesion force on the SiO_2 surface, followed by the TiO_2 and Al_2O_3 surfaces, respectively. The adhesion force between silicon nitride AFM tips and the five humic coated sample surfaces increased in the order mica < Fe_2O_3 < Al_2O_3 < TiO_2 < SiO_2. With the exception of mica, all coated surfaces experienced a greater standard deviation than their uncoated counterparts. The standard deviation of the coated surfaces increased in the order mica < Al_2O_3 ≈ Fe_2O_3 < TiO_2 ≈ SiO_2. With the exception of TiO_2 and Al_2O_3, the standard deviations of the uncoated surfaces were roughly the same.

At long residence times, humic acid coating increased the sticky (F_5) adhesion force on all surfaces except Fe_2O_3 (Figure 4.3b). The largest increase in adhesion force was observed for SiO_2, followed by Al_2O_3, TiO_2, and mica, respectively. Humic acid adsorption resulted in an increase in standard deviation for all surfaces in comparison to the uncoated surfaces. The adhesion force between silicon nitride AFM tips and the five humic coated sample surfaces increased in the order mica < Fe_2O_3 < SiO_2 < TiO_2 < Al_2O_3.

The standard deviation of the coated surfaces increased in the order mica < Fe_2O_3 < TiO_2 ≈ SiO_2 < Al_2O_3. The standard deviation of the uncoated surfaces increased in the order mica < Fe_2O_3 < TiO_2 < Al_2O_3 < SiO_2.

Humic acid adsorption decreased the adhesion force on mica except at long residence times at localized, sticky sites (Figure 4.4a). When analyzing the average force spectra, adhesion to humic acid-coated mica was less than that to uncoated mica at the same residence time. However, when considering the sticky forces, adhesion to the coated surface was less than that to the uncoated surface only at a zero second residence time. At residence times of one and ten seconds, adhesion to the coated surface exceeded that to the uncoated surface. In all cases increased tip-surface residence time correlated positively with adhesion force. The standard deviation of the coated surface also increased with residence time, but no trend was observed for the uncoated surface.

Al_2O_3 behaved differently than mica because at all residence times adhesion to the coated surface exceeded that to the uncoated surface (Figure 4.4b). The coated surface proved stickier than the uncoated one whether the average or sticky forces were analyzed. Furthermore, the standard deviation generally increased with residence time, and the standard deviation of the coated surface was greater than that of the uncoated surface.

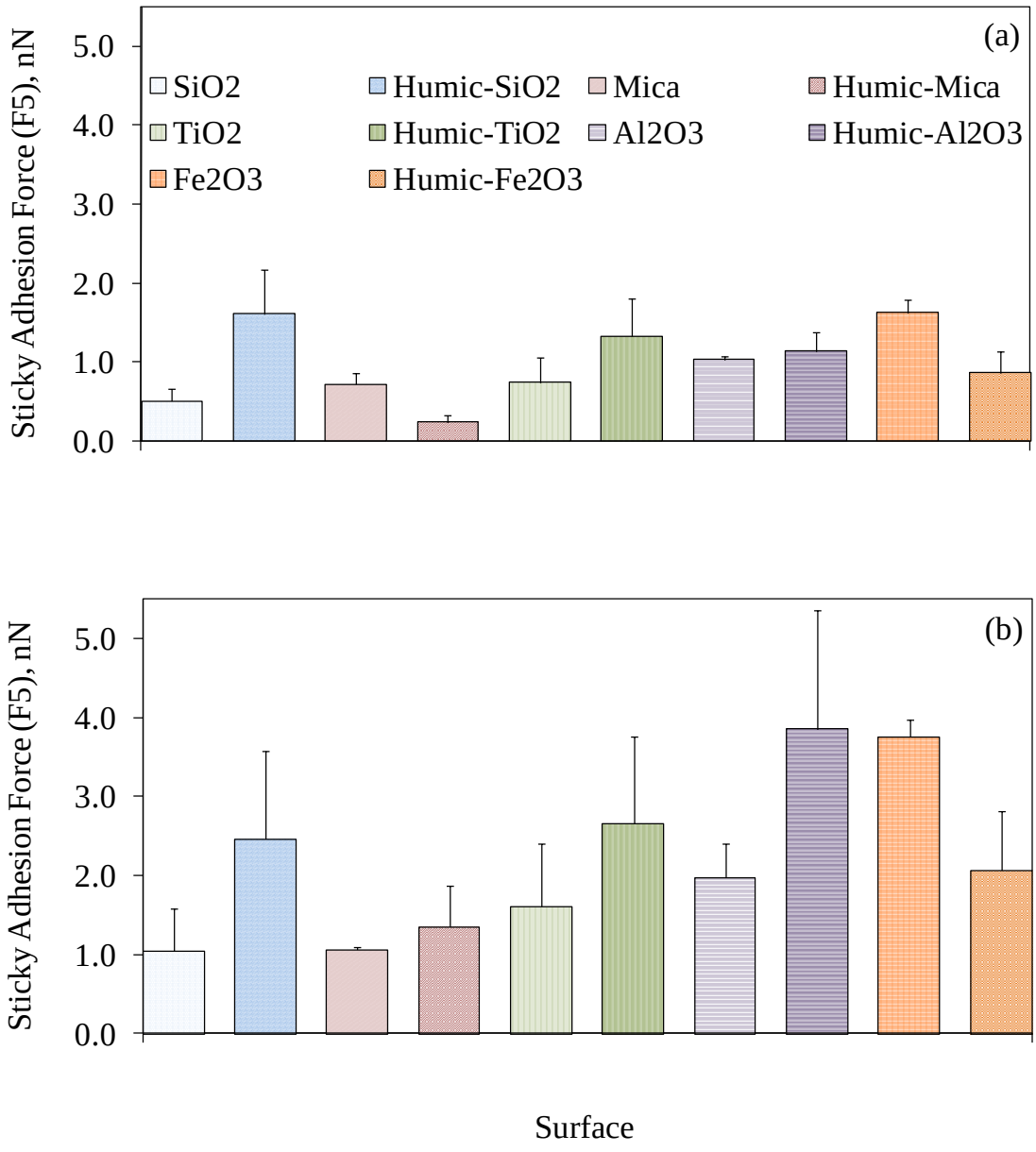

Figure 4.3: Sticky adhesion forces (F_5) on uncoated and humic acid-coated surfaces at (a) short (zero seconds) and (b) long (10 seconds) residence times.

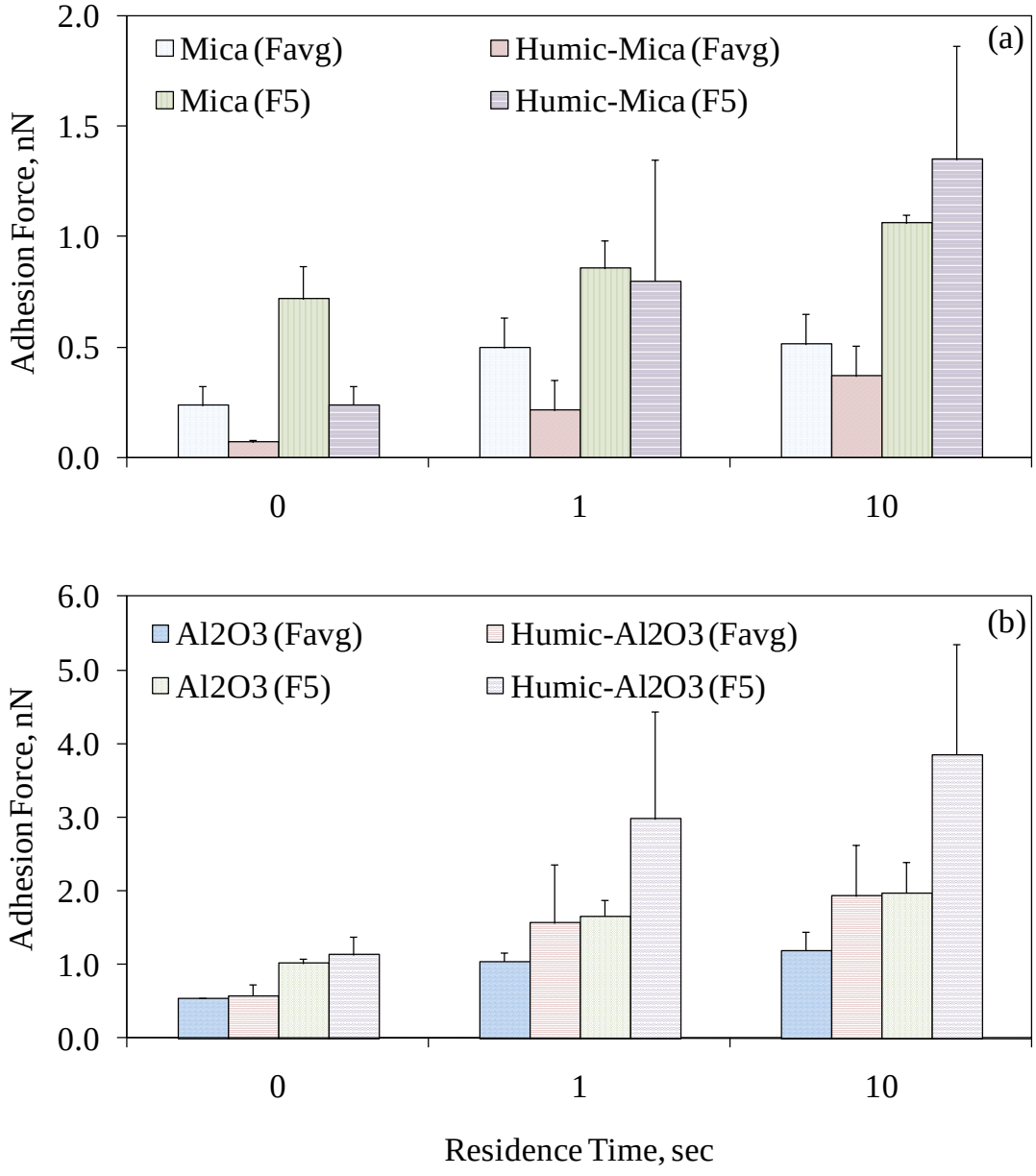

Figure 4.4: Adhesion forces on (a) uncoated and humic acid-coated mica and (b) uncoated and humic acid-coated Al_2O_3 as a function of residence time.

4.2 Spectral Force Analysis (SFA)

Spectral force analysis curves provided an alternative means of visualing the distribution of adhesion forces on the uncoated and humic acid-coated surfaces as a function of residence time (Figure 4.5). The shape of the spectral force curve provides insight into the distribution of adhesion forces and thus a qualitative measure of surface heterogeneity. Curves with steep slopes indicate a relative uniform distribution of adhesion force between the sample surface and AFM tip, while curves with flattened slopes indicate more adhesion force variability. For instance, a vertical line indicates the improbable scenario where all the measured forces are identical.

At short residence times, the uncoated and humic-coated SiO_2 surfaces exhibited the greatest variability (Figure 4.5a). As evidenced by the total cumulative force, humic-coated SiO_2 had the highest average adhesion force, followed by the uncoated Fe_2O_3 surface. Humic-coated SiO_2 also had the greatest sticky force, as observed by the relatively small number of high adhesion events. Uncoated SiO_2 had the second lowest average adhesion force, with only humic-coated mica having a lower average force. There was very little difference between the uncoated and humic-coated Al_2O_3 surfaces, as evidenced by the minimal spread between the two curves. The shapes of the uncoated and humic-coated TiO_2 curves are similar, but the humic-coated surface has a noticeably higher average adhesion force as observed by the upward translation of the curve.

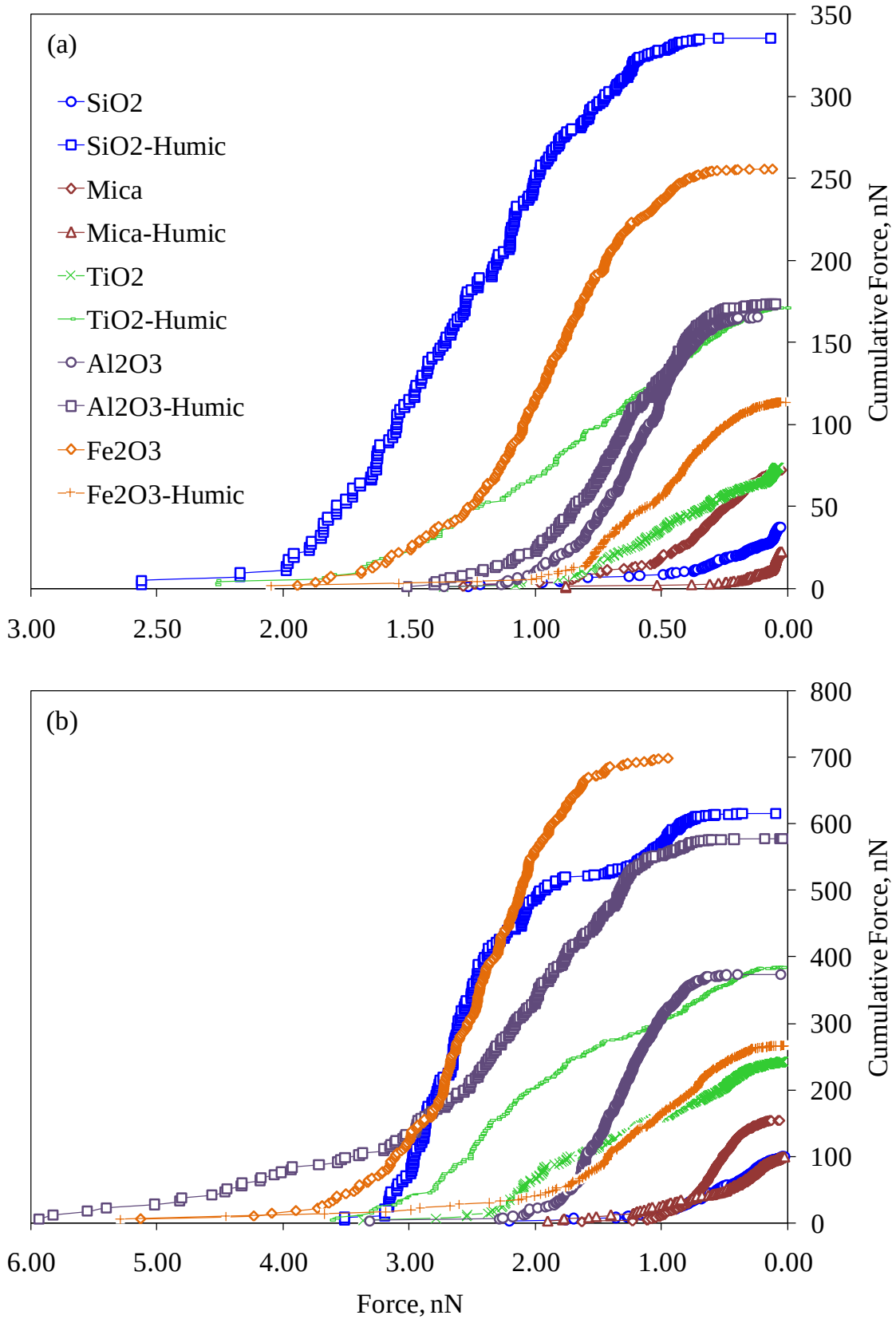

Figure 4.5: Spectral force curves for uncoated and humic acid-coated surfaces at (a) short (t = 0 seconds) and (b) long (t = 10 seconds) residence times.

At long residence times, the uncoated Fe_2O_3 surface exhibited the largest average adhesion force, followed by the humic-coated SiO_2 and humic-coated Al_2O_3 surfaces, respectively (Figure 4.5b). The humic-coated Al_2O_3 surface had the largest sticky force, as observed by the long tail of the curve in the high force range. Uncoated and humic-coated mica as well as uncoated SiO_2 dominated the lower end of the force range. Uncoated and humic-coated TiO_2 again exhibited a relatively uniform distribution of adhesion forces, as observed by their linear shape in comparison to the other curves. In general, the relative shapes of the spectral force curves at long residence times are similar to the curves at short residence times. The main difference with the curves at long residence times is that their tails extend into the higher force range and their total cumulative force is greater than their counterparts at lower residence times.

Uniformity of the calculated adhesion forces generally decreased following humic acid adsorption (Table 4.1). With the exception of mica at short residence times (t=0), the Weibull standard deviation incrased at both long and short residence times in the presence of humic acid.

Table 4.1: Weibull Standard Deviation of Adhesion Forces as a Function of Sample Surface and Residence Time

	Residence Time (sec)			**Residence Time (sec)**	
Uncoated Surface	**0**	**10**	**Coated Surface**	**0**	**10**
Mica	0.0670	0.0699	Mica	0.0422	0.0913
Al_2O_3	0.0556	0.0790	Al_2O_3	0.0871	0.2717
Fe_2O_3	0.0892	0.0880	Fe_2O_3	0.0981	0.1946
SiO_2	0.0311	0.0990	SiO_2	0.1080	0.2704
TiO_2	0.0732	0.2267	TiO_2	0.1518	0.3073

Note: Standard deviation in units of nanonewtons (nN)

4.3 Topographical Imaging Results

4.3.1 Uncoated Surface Characterization

Topographical images of the uncoated surfaces provide a baseline for comparison to the humic acid-coated surfaces (Figures 4.6a,c to 4.10a,c). Surfaces were imaged with one micron and five micron scan sizes in order to provide a better depiction of both isolated and overall surface features. Mica appeared to be the smoothest surface analyzed, as evidenced by the absence of any surface features over both a one micron and five micron scan size. Surface features were visible on the other four surfaces. Al_2O_3 appeared to be the most heterogeneous of the uncoated surfaces. It was difficult to differentiate between uncoated SiO_2, TiO_2, and Fe_2O_3 based solely on the topographical images.

4.3.2 Effect of Humic Acid Adsorption on Surface Characterization

Humic acid adsorption produced noticeable surface features on all five surfaces (Figures 4.6b,d to 4.10b,d). Images of coated surfaces differed from those of uncoated surfaces for both one and five micron scan sizes. In all cases the visible surface features on the coated surfaces were greater in number and larger in size than those on the uncoated surfaces.

4.3.3 Effect of Humic Acid Adsorption on Surface Roughness

Root mean square (RMS) surface roughness of the uncoated surfaces increased in the order $TiO_2 < Fe_2O_3 <$ mica $< SiO_2 < Al_2O_3$ at both one micron and five micron scan sizes (Table 4.2). The coated surfaces exhibited a different trend of surface roughness

than the uncoated surfaces. Specifically, the RMS surface roughness of the coated surfaces increased in the order mica < TiO_2 < SiO_2 < Fe_2O_3 < Al_2O_3 and mica < SiO_2 < Fe_2O_3 < TiO_2 < Al_2O_3 at one micron and five micron scan sizes, respectively. Humic acid adsorption generally increased the roughness of the coated surfaces; however, the surface roughness of mica actually decreased following humic acid adsorption at both one micron and five micron scan sizes. SiO_2 surface roughness also decreased after humic acid adsorption at a scan size of five microns.

Table 4.2: Roughness of Uncoated and Humic Acid-Coated Surfaces

	Scan Size (μm)			**Scan Size (μm)**	
Uncoated Surface	**1**	**5**	**Coated Surface**	**1**	**5**
TiO_2	1.45 nm	1.95 nm	TiO_2	3.57 nm	9.65 nm
Fe_2O_3	1.99 nm	3.52 nm	Fe_2O_3	9.64 nm	5.41 nm
Mica	3.38 nm	4.48 nm	Mica	3.11 nm	1.06 nm
SiO_2	4.24 nm	5.33 nm	SiO_2	5.64 nm	4.08 nm
Al_2O_3	8.64 nm	10.7 nm	Al_2O_3	10.1 nm	11.0 nm

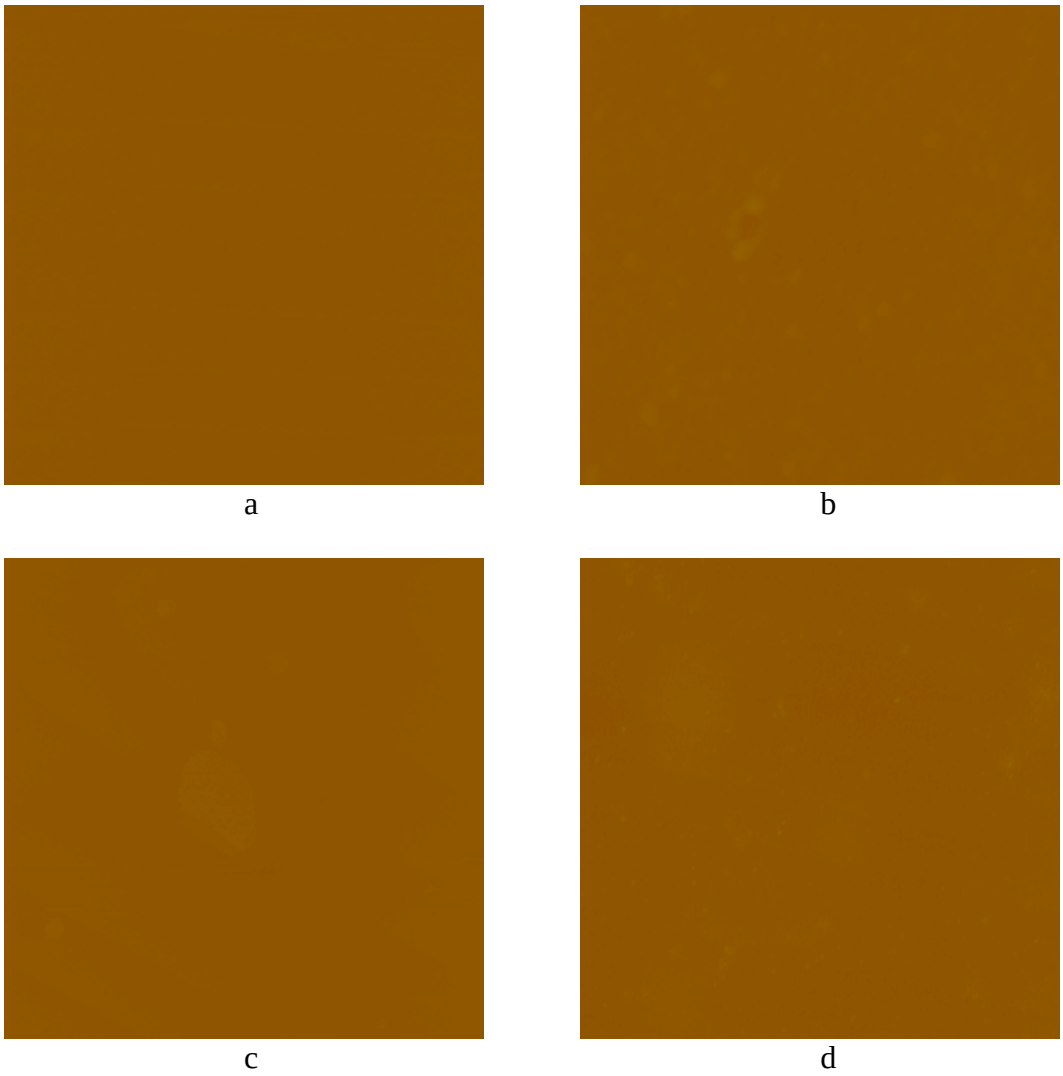

Figure 4.6: Topographical image of (a) uncoated mica and (b) humic acid-coated mica over a 1-μm scan area, and (c) uncoated mica and (d) humic acid-coated mica over a 5-μm scan area.

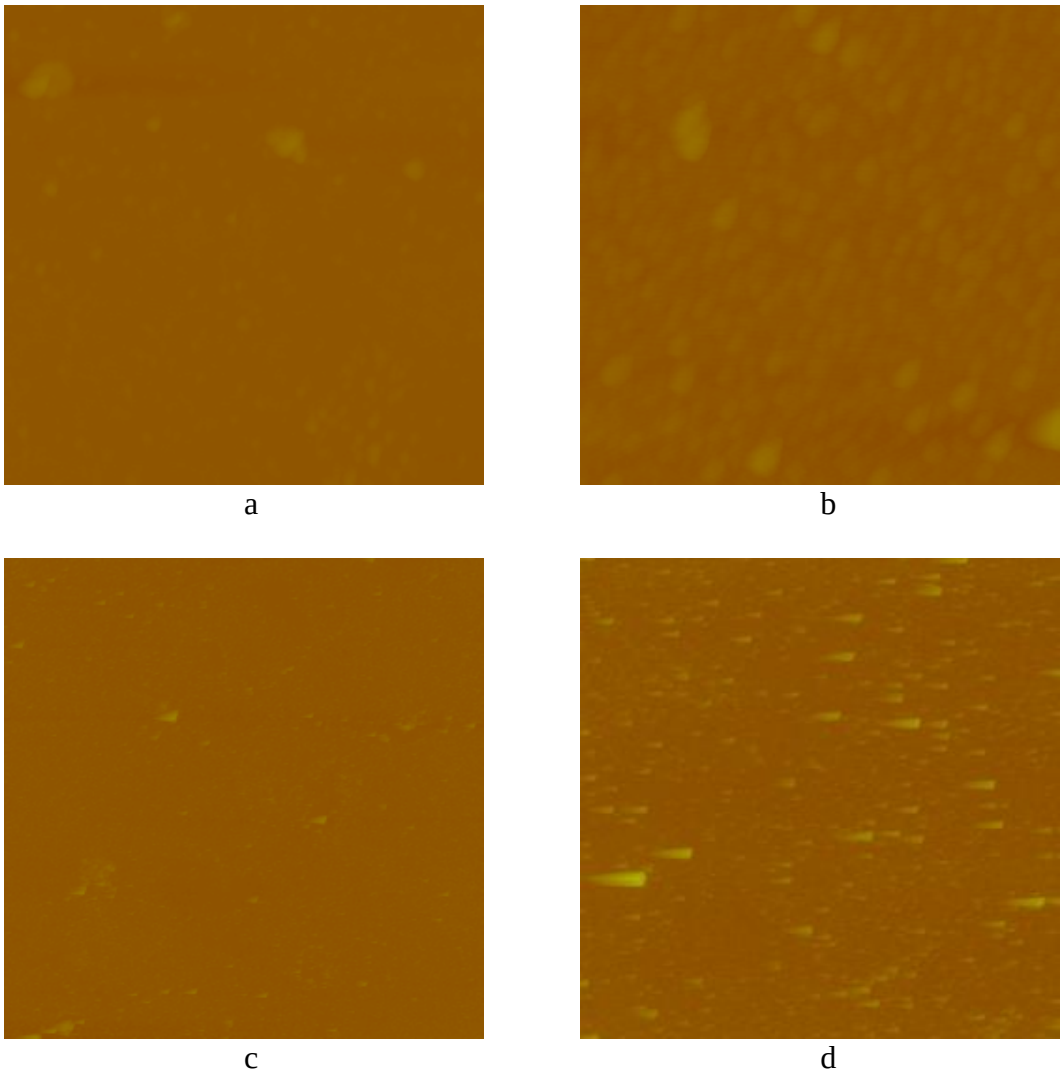

Figure 4.7: Topographical image of (a) uncoated SiO_2 and (b) humic acid-coated SiO_2 over a 1-μm scan area, and (c) uncoated SiO_2 and (d) humic acid-coated SiO_2 over a 5-μm scan area.

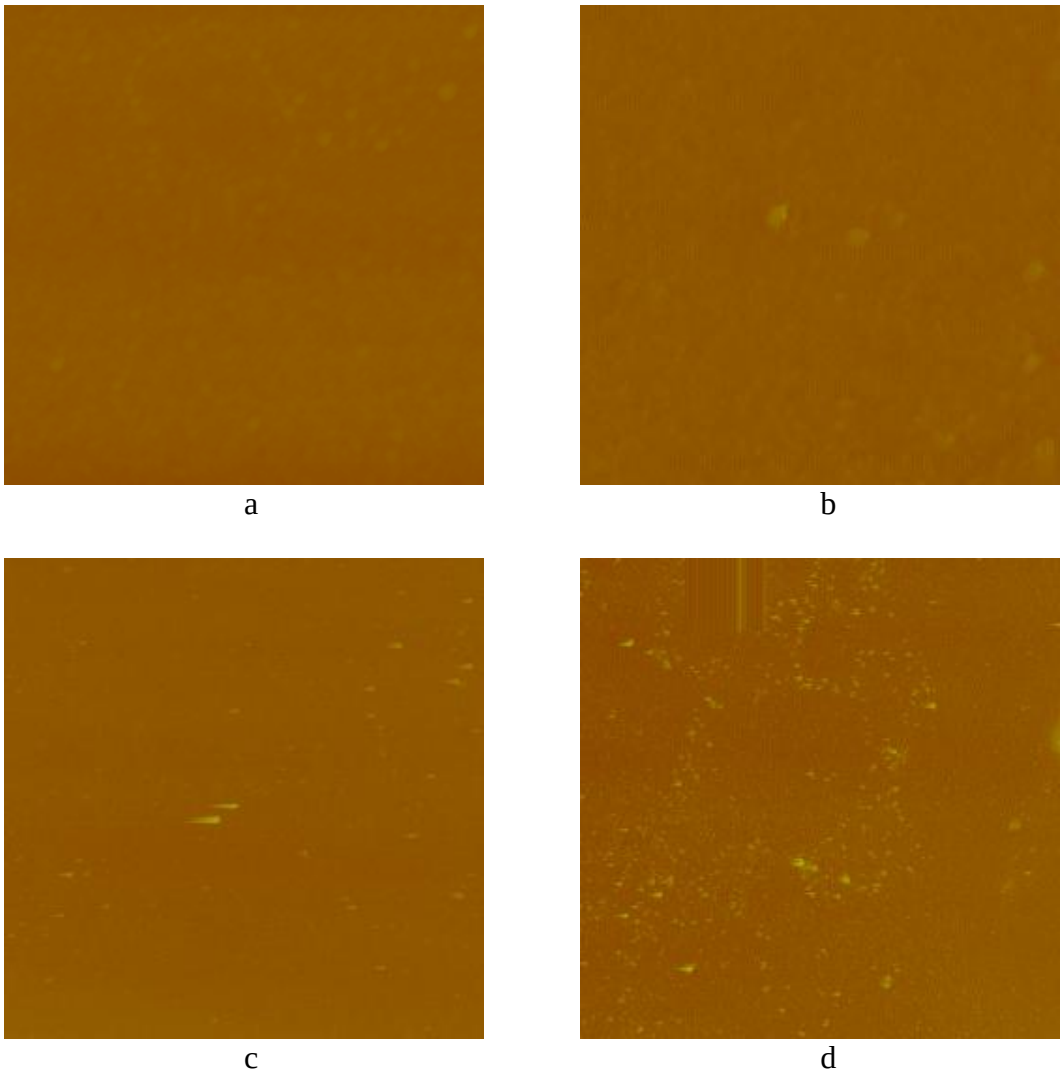

Figure 4.8: Topographical image of (a) uncoated TiO_2 and (b) humic acid-coated TiO_2 over a 1-μm scan area, and (c) uncoated TiO_2 and (d) humic acid-coated TiO_2 over a 5-μm scan area.

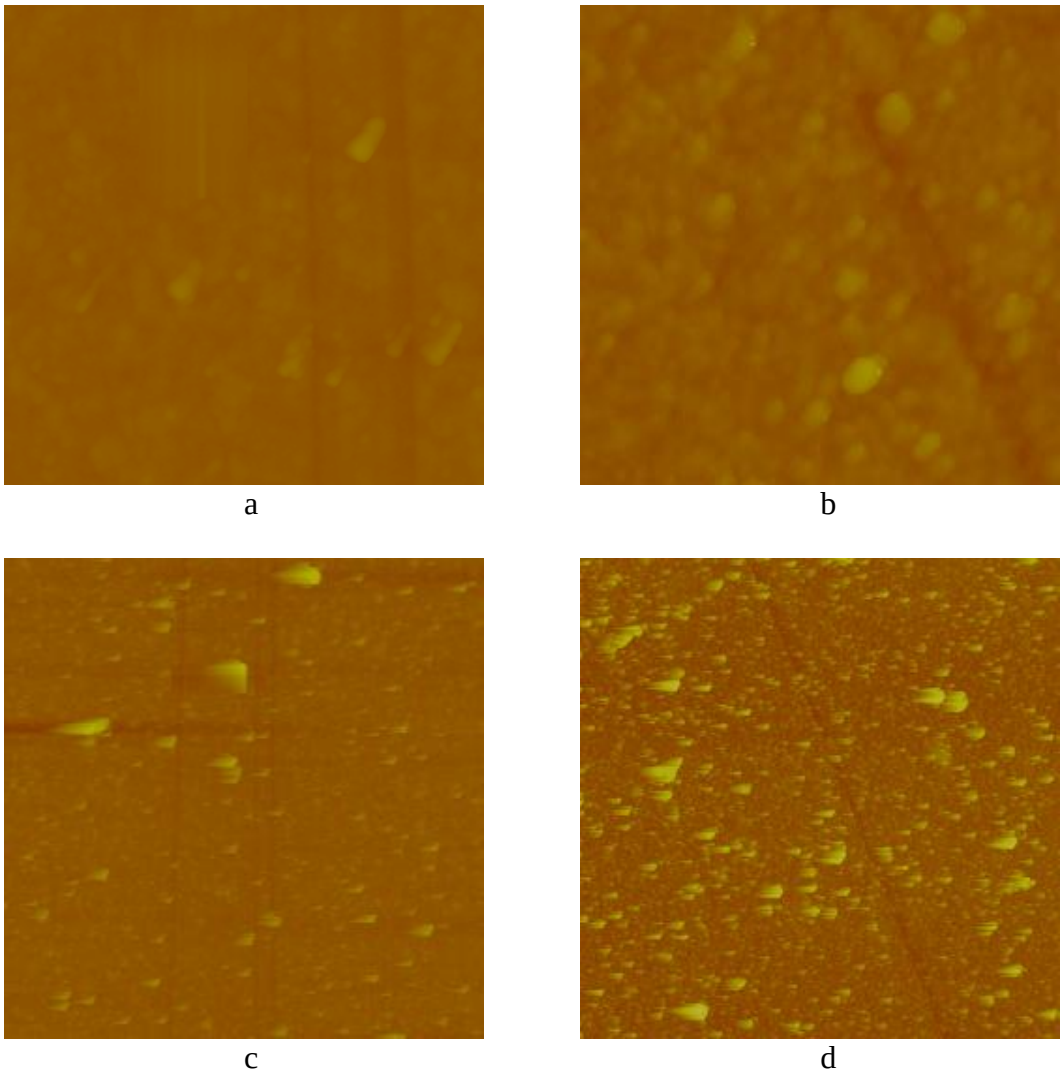

Figure 4.9: Topographical image of (a) uncoated Al_2O_3 and (b) humic acid-coated Al_2O_3 over a 1-μm scan area, and (c) uncoated Al_2O_3 and (d) humic acid-coated Al_2O_3 over a 5-μm scan area.

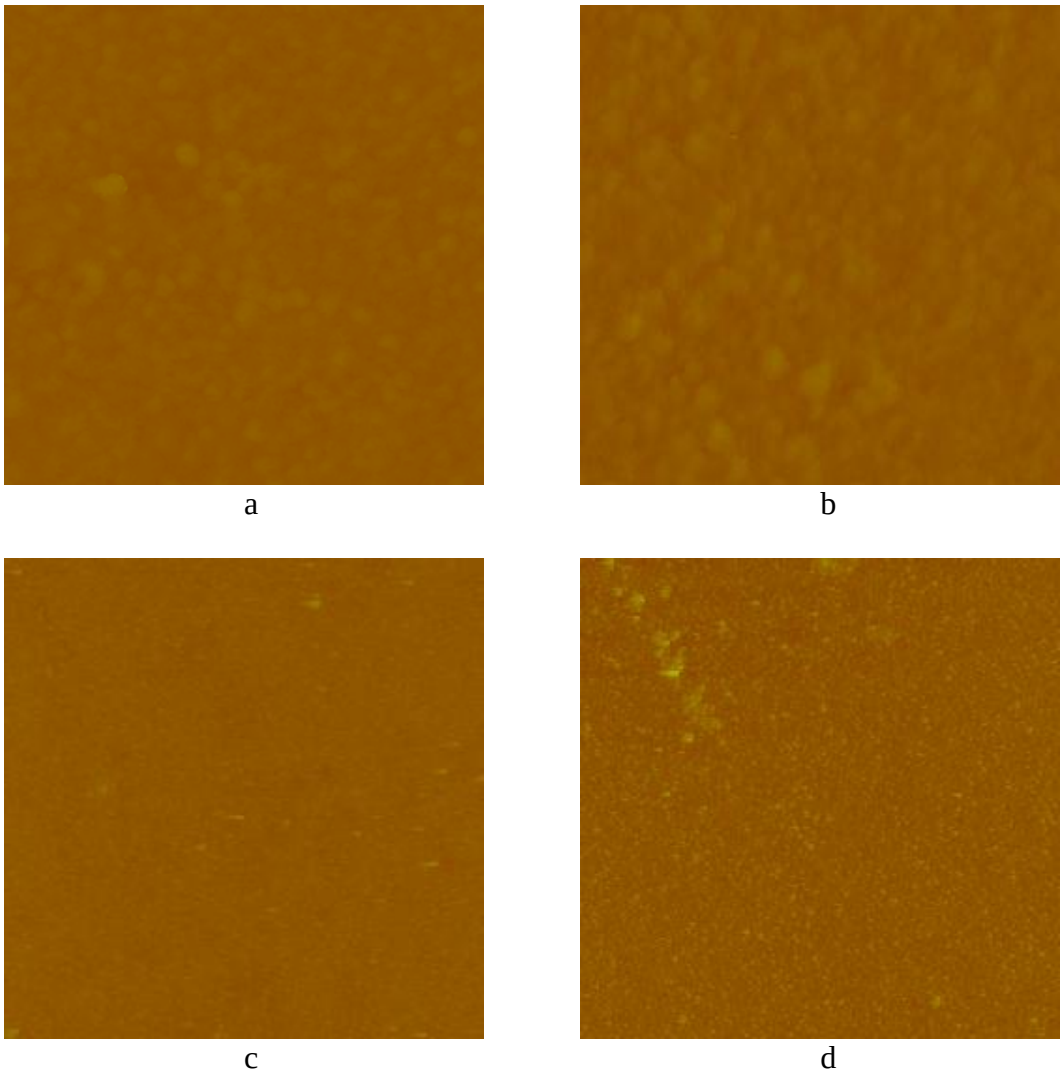

Figure 4.10: Topographical image of (a) uncoated Fe_2O_3 and (b) humic acid-coated Fe_2O_3 over a 1-μm scan area, and (c) uncoated Fe_2O_3 and (d) humic acid-coated Fe_2O_3 over a 5-μm scan area.

5 DISCUSSION

5.1 Adhesion to Uncoated Surfaces

Adhesion between the silicon nitride AFM tip and uncoated surfaces increased in the order SiO_2 < mica < TiO_2 < Al_2O_3 < Fe_2O_3, regardless of whether the average (F_{avg}) or sticky (F_5) forces were analyzed. The purpose of examining the uncoated surfaces was to create a baseline for comparison to the surfaces to which humic acid was adsorbed. The reported results are consistent with both macroscale adhesion tests utilizing various strains of bacteria (Li and Logan, 2004) and nanoscale AFM experiments (Vadillo-Rodríguez and Logan, 2006). Li and Logan (2004) conducted macroscale adhesion tests using eight bacterial strains and eleven surfaces, including the same metal oxide surfaces used in the present study. Vadillo-Rodríguez and Logan (2006) conducted nanoscale AFM experiments using regular silicon nitride and latex microsphere colloid probes, also examining the same surfaces. The results of both studies indicated that adhesion to the metal oxide surfaces increased in the order SiO_2 < TiO_2 < Al_2O_3 < Fe_2O_3 (mica was not analyzed in either of these studies).

Comparison of the adhesion results and surface roughness measurements suggests surface roughness is not the single most important determinant of the relative adhesion between the uncoated surfaces. If adhesion depended primarily on surface roughness, adhesion force should have increased in the order TiO_2 < Fe_2O_3 < mica < SiO_2 < Al_2O_3 based on the results of this work. The results of Li and Logan (2004) and Vadillo-Rodríguez and Logan (2006) support the same hypothesis, but Shellenberger and Logan (2002) demonstrated a stronger correlation between surface roughness and bacterial

adhesion when filtering latex microspheres (bacterial surrogates) through columns containing chemically treated rough and smooth glass beads. However, it is important to note that in the study by Shellenberger and Logan, the surface roughness of the rough and smooth beads was approximately 38 nm and 15 nm, respectively, which is one order of magnitude higher than the surface roughness of the uncoated and coated surfaces utilized in the current study (Al_2O_3 being the sole exception).

5.2 Effect of Residence Time on Adhesion

Adhesion force between the AFM tip and the uncoated surfaces correlated positively with tip-surface residence time, irrespective of whether the average or sticky forces were considered. Residence time affected the magnitude of the adhesion force but not the relative stickiness of the surfaces. Regardless of residence time, adhesion force between the AFM tip and uncoated surfaces increased in the order SiO_2 < mica < TiO_2 < Al_2O_3 < Fe_2O_3. In all cases the increase in adhesion between zero and one second residence times exceeded the increase in adhesion between one and ten second residence times, suggesting the adhesion force approaches a plateau after a certain amount of contact time.

5.3 Effect of Humic Acid Adsorption on Adhesion

At short residence times (i.e. zero seconds) humic acid adsorption resulted in an increase in adhesion force on all surfaces except mica and Fe_2O_3, irrespective of whether the average forces (F_{avg}) or sticky forces (F_5) were analyzed. With the exception of mica and Fe_2O_3, this result is contrary to the hypothesis that humic acid adsorption to metal

oxide surfaces will preferentially occur at surface sites in order of decreasing stickiness, and that the net effect of this adsorption will produce a modified surface less favorable for adhesion to the AFM tip. The results for bacterial adhesion would depend on whether bacteria stick more or less to humics compared to the AFM tip.

At long residence times (i.e. ten seconds) humic acid adsorption resulted in an increase in adhesion force on all surfaces except mica and Fe_2O_3 when considering the average forces. When considering the sticky forces, humic acid adsorption resulted in an increase in adhesion force on all surfaces except Fe_2O_3. With the exception of the average force on mica and Fe_2O_3 and the sticky force on Fe_2O_3, these results are consistent with the hypothesis that in the presence of humic acids, the adhesion force at long residence times exceeds that of the uncoated surface at the same residence time.

Surface roughness was a better predictor of adhesion force in consideration of the humic-coated surfaces than the uncoated surfaces. At long residence times, surface roughness at a five micron scan size generally correlated with both the average and sticky adhesion force on the humic-coated surfaces, with the exception of SiO_2. The RMS surface roughness of the coated surfaces at five micron scan sizes increased in the order mica < SiO_2 < Fe_2O_3 < TiO_2 < Al_2O_3. At long residence times, the sticky and average adhesion forces on the humic-coated surfaces (excluding SiO_2) increased in the order mica < Fe_2O_3 < TiO_2 < Al_2O_3. At short residence times the correlation between surface roughness and adhesion force was weaker because the sticky and average adhesion forces on the humic-coated surfaces (excluding SiO_2) increased in the order mica < Fe_2O_3 < Al_2O_3 < TiO_2 and mica < Fe_2O_3 < $TiO_2 \approx Al_2O_3$, respectively.

In general, humic acid adsorption resulted in an increase in surface roughness, which is consistent with the Weibull standard deviation results suggesting uniformity of the calculated adhesion forces decreased following humic adsorption. Surface roughness and adhesion force uniformity are not synonymous, but one can argue that a rough surface has the potential for more heterogeneity with regards to adhesion sites, thus explaining the decrease in force uniformity following humic adsorption.

The point of zero charge (pH_{zpc}) of mica, TiO_2, Fe_2O_3, and Al_2O_3 is approximately 6.6, 6.2, 6.8, and 9.1, respectively, so all four surfaces are positively charged under the experimental conditions (i.e. solution pH ≈ 4.5) (Table 5.1). SiO_2 (pH_{zpc} ≈ 2.0) is negatively charged under the experimental conditions because it has a pH_{zpc} value less than the pH of the experimental background solution. However, at both long and short residence times in consideration of both the average and sticky forces, SiO_2, Ti_2O_2, and Al_2O_2 behaved similarly. Mica and Fe_2O_3 generally exhibited the opposite trend, the one exception being the sticky adhesion force on mica at long residence times.

Table 5.1: Point of Zero Charge (pH_{zpc}) of Uncoated Surfaces

Material	**pH_{zpc}**
SiO_2	2.0
Mica	6.6
TiO_2	6.2
Fe_2O_3	6.8
Al_2O_3	9.1

Source: Vadillo-Rodríguez (2004)

Humic acid ($pH_{zpc} \approx 4.0$) is negatively charged under the experimental conditions (pH ≈ 4.5), so it should readily adsorb to the four positively charge surfaces, creating a modified surface with a negative charge. The silicon nitride AFM tip ($pH_{zpc} \approx 7.5$) is positively charged under the experimental conditions. Therefore, in the case of the TiO_2 and Al_2O_3 surfaces, the increase in adhesion force following humic acid adsorption can possibly be explained by electrostatics. However, this explanation does not account for the behavior of mica and Fe_2O_3, the other two positively charged surfaces. Perhaps in the case of mica and Fe_2O_3, the underlying surface has a greater impact on the adhesion force than the adsorbed humic acid; however, even if this was the case, it is difficult to explain why the adhesion force decreased on mica and Fe_2O_3 in the presence of the humic acid.

The increase in adhesion force on the SiO_2 surface in the presence of humic acid can be explained by electrostatics assuming humic acid did in fact adsorb to the surface (i.e. positively charged AFM tip interacting with negatively charged humic acid), but the reason for the humic acid adsorption is not clearly understood (i.e. negatively charged humic acid interacting with negatively charged surface). SiO_2 is negatively charged under the experimental conditions, but it behaved similarly to the positively charged TiO_2 and Al_2O_3 surfaces. Negatively charged humic acid should have exhibited a weak electrostatic attraction to the SiO_2 surface; however, comparison of the topographical images of the uncoated and humic acid-coated SiO_2 surfaces indicates that humic acid appeared to readily adsorb to the SiO_2 surface.

Comparison of the AFM force data and topographical images before and after humic adsorption suggests that humic material readily adsorbed to each of the five sample surfaces, but the amount of adsorption was not directly quantified as part of this

research. Murphy et al. (1990) conducted adsorption experiments with peat humic acid and Suwannee River humic acid on hematite and kaolinite, and adsorption to hematite was greater than that to kaolinite with respect to both humic acids. This finding appears to contrast with the electrostatics arguments made earlier as well as the observation presented in this work that adhesion to Al_2O_3 was greater than that to Fe_2O_3 following humic acid adsorption. Yang et al. (2009) found that the amount of peat humic acid adsorbed to various inorganic oxides increased in the order α-Al_2O_3 < ZnO < TiO_2 < γ-Al_2O_3, which is consistent with the observation from the present research of a larger increase in adhesion force on Al_2O_3 than TiO_2 following humic adsorption. Interestingly, in this same work the researchers were unable to adsorb humic material on SiO_2, consistent with electrostatic arguments. Other investigators have successfully used AFM to image large humic acid globules adsorbed to mica under a variety of conditions, consistent with the AFM force data presented herein suggesting a relatively large difference in the measured adhesion force before and after humic adsorption on mica (Liu et al., 2000; Balnois et al., 1999).

The configuration of adsorbed humic material may also influence adhesion events, and although quantifying humic structure was beyond the scope of this research, some general conclusions can nonetheless be established between humic structure and solution ionic strength. It is generally agreed that bacterial adhesion increases with ionic strength, the idea being that the thickness of the repulsive layer between the two surfaces increases as ionic strength decreases (Xu et al., 2005; Li and Logan, 1999; Zita and Hermansson, 1994). However, the presence of adsorbed humic material on a mineral or other substrate complicates this simple model. Murphy et al. (1992 and 1994) demonstrated that

adhesion to humic material is inversely proportional to the ionic strength of solution. In high ionic strength solution humic acids tend to coil up, resulting in less surface area available for adhesion, while in low ionic strength solution humic acids adopt a more open configuration that is more conducive for adhesion. The ultrapure water used in the present adhesion experiments had a relatively low ionic strength, so it can be assumed that the adsorbed humic material adopted a more open configuration.

5.4 Spectral Force Analysis (SFA)

Spectral force analysis (SFA) provided an alternative means for analyzing the interaction of the AFM tip and the sample surfaces. SFA was introduced as a useful tool for analyzing the distribution of adhesion forces on a surface by simultaneously providing insight into the effect of humic acid adsorption, residence time, and the small number of highly sticky surface sites. The shape of an SFA curve sheds light on the type of force distribution. For instance, curves that stretch out horizontally indicate a high degree of force variability, while curves with steep slopes suggest a more uniform force distribution. When plotting multiple curves on one graph, comparison of the average adhesion forces (F_{avg}) is accomplished by comparing the cumulative force for each curve (i.e. the average adhesion force is in direct proportion to the cumulative force). Similarly, curves that stretch horizontally into the high force range result in correspondingly higher sticky forces (F_5).

5.5 Future Experiments

In the future it might be interesting to refine the experimental conditions to better represent bacterial adhesion in natural environments. For instance, it would make sense to modify the AFM probe so that it is negatively charged like most bacteria. The AFM probe can be given a negative charge by bonding a colloid that exhibits a negative charge under the experimental conditions to the end of a tipless cantilever. Commonly used colloids include glass and latex microspheres of varying sizes. Alternatively, a single bacterium could be affixed to the end of the cantilever. Bacterial adhesion studies such as column experiments in the presence and absence of humics could be compared with AFM results. Furthermore, it might be useful to conduct future experiments in a PIPES buffer solution to provide better control of the experimental pH.

6 CONCLUSIONS

The purpose of this research was to mimic bacterial adhesion to metal oxide surfaces in the presence of natural organic matter using atomic force microscopy (AFM). Adhesion forces between the uncoated surfaces and standard silicon nitride AFM probes increased in the order SiO_2 < mica < TiO_2 < Al_2O_3 < Fe_2O_3, regardless of whether the average (F_{avg}) or sticky (F_5) forces were analyzed. Increasing the tip-surface residence time increased the adhesion force, but did not change the relative order of the surfaces. At short residence times humic acid adsorption resulted in an increase in adhesion force on all surfaces except mica and Fe_2O_3, irrespective of whether the average forces (F_{avg}) or sticky forces (F_5) were analyzed. At long residence times humic acid adsorption resulted in an increase in adhesion force on all surfaces except mica and Fe_2O_3 when considering the average forces. When considering the sticky forces at long residence times, humic acid adsorption resulted in an increase in adhesion force on all surfaces except Fe_2O_3.

No consistent explanation could account for the observed results, although arguments based on electrostatics and surface roughness could explain the tip-surface interaction in certain instances. Spectral force analysis was introduced as an alternative means of analyzing the interaction between AFM probes and sample surfaces. It was concluded that standard silicon nitride AFM probes are not ideal bacterial surrogates, so further work with colloid AFM and other bacterial deposition studies is needed to better understand bacterial adhesion to metal oxides in the presence of natural organic matter.

REFERENCES

Absolom, D. R.; Lamberti, F. V.; Policova, Z.; Zingg, W.; van Oss, C. J.; and Neumann, A. W. "Surface thermodynamics of bacterial adhesion." *Applied and Environmental Microbiology* **1983**, 46 (1), 90-97.

Baier, R. E. "Conditioning surfaces to suit the biomedical environment: recent progress." *Journal of Biomechanical Engineering* **1982**, 104, 257-271.

Balnois, E.; Wilkinson, K. J.; Lead, J. R.; and Buffle, J. "Atomic Force Microscopy of Humic Substances: Effects of pH and Ionic Strength." *Environmental Science and Technology* **1999**, 33, 3911-3917.

Bell, C. H.; Arora, B. S.; and Camesano, T. A. "Adhesion of *Pseudomonas putida* KT2442 is mediated by surface polymers at the nano- and microscale." *Environmental Engineering Science* **2005**, 22 (5), 629-641.

Bentham, R. H. "Environmental factors affecting the colonization of cooling towers by Legionella spp. in South Australia." *International Biodeterioration and Biodegradation* **1993**, 31, 55-63.

Binnig, G. and Rohrer, H. "Surface Imaging by Scanning Tunneling Microscopy." *Ultramicroscopy* **1983**, 11 (2-3), 157-160.

Binnig, G., Quate, C. F., and Gerber, Ch. "Atomic Force Microscope." *Physical Review Letters* **1986**, 56 (9), 930-933.

Bouttier, S.; Han, K. G.; Ntsama, C.; Bellon-Fontaine, M. N.; and Fourniat, J. "Role of electrostatic interactions in the adhesion of *Pseudomonas fragi* and *Brochothrix thermosphacta* to meat." *Colloids and Surfaces B: Biointerfaces* **1994**, 2, 57-65.

Bruinsma, G. M.; van der Mei, H. C.; Busscher, H. J. "Bacterial adhesion to surface hydrophilic and hydrophobic contact lenses." *Biomaterials* **2001**, 22, 3217-3224.

Butt, H.-J., Cappella, B., and Kappl, M. "Force measurements with the atomic force microscope: Technique, interpretation, and applications." *Surface Science Reports* **2005**, 59, 1-152.

Camesano, T. A. and Logan, B. E. "Influence of fluid velocity and cell concentration on the transport of motile and nonmotile bacteria in porous media." *Environmental Science and Technology* **1998**, 32 (11), 1699-1708.

Cleveland, J. P.; Manne, S.; Bocek, D.; and Hansma, P. K. "A nondestructive method for determining the spring constant of cantilevers for scanning force microscopy." *Review of Scientific Instruments* **1993**, 64 (2), 403-405.

Clint, J. H. and Wicks, A. C. "Adhesion under water: surface energy considerations." *International Journal of Adhesion and Adhesives* **2001**, 21, 267-273.

Dempsey, M. J. "Marine bacterial fouling: A scanning electron microscope study." *Marine Biology* **1981**, 61 (4), 305-315.

Dufrêne, Y. F. "Atomic force microscopy, a powerful tool in microbiology." *Journal of Bacteriology* **2002**, 184 (19), 5205-5213.

Gamby, J.; Pailleret, A.; Clodic, C. B.; Pradier, C.-M.; Tribollet, B. "In situ detection and characterization of potable water biofilms on materials by microscopic, spectroscopic, and electrochemistry methods." *Electrochimica Acta* **2008**, 54, 66-73.

Gexin, C. and Walker, S. L. "Role of solution chemistry and ion valence on the adhesion kinetics of groundwater and marine bacteria." *Langmuir* **2007**, 23 (13), 7162-7169.

Gottenbos, B.; van der Mei, H. C.; Busscher, H. J.; Grijpma, D. W.; and Feijen, J. "Initial adhesion and surface growth of *Pseudomonas aeruginosa* on negatively and positively charged poly(methacrylates)." *Journal of Materials Science: Materials in Medicine* **1999**, 10, 853-855.

Hilal, N.; Al-Khatib, L.; Atkin, B. P.; Kochkodan, V.; and Potapchenko, N. "Photochemical modification of membrane surfaces for (bio)fouling reduction: a nano-scale study using AFM." *Desalination* **2003**, 158, 65-72.

Hilal, N.; Mohammad, A. W.; Atkin, B.; and Darwish, N. A. "Using atomic force microscopy towards improvement in nanofiltration membranes properties for desalination pre-treatment: a review" *Desalination* **2003**, 137-144.

Hutter, J. L. and Bechhoefer, J. "Calibration of atomic-force microscope tips." *Review of Scientific Instruments* **1993**, 64 (7), 1868-1873.

Jagels, R.; Murdoch, C. W.; Pietroski, J.; and Carlisle, J. "In situ bacterial assay for two plywood adhesives." *Forest Products Journal* **1995**, 45 (9), 51-54.

Jalili, N. and Karthik, L. "A review of atomic force microscopy imaging systems: application to molecular metrology and biological sciences." *Mechatronics* **2004**, 14, 907-945.

Li, B. and Logan, B. E. "Bacterial adhesion to glass and metal-oxide surfaces." *Colloids and Surfaces B: Biointerfaces* **2004**, 36, 81-90.

Li, Q. and Logan, B. E. "Enhancing bacterial transport for bioaugmentation of aquifers using low ionic strength solutions and surfactants." *Water Resources* **1999**, 33 (4), 1090-1100.

Liu, A.; Wu, R. C.; Eschenazi, E.; and Papadopoulos, K. "AFM on humic acid adsorption on mica." *Colloids and Surfaces A: Physicochemical and Engineering Aspects* **2000**, 174, 245-25.

Ma, H.; Winslow, C. J.; and Logan, B. E. "Spectral force analysis using atomic force microscopy reveals the importance of surface heterogeneity in bacterial and colloid adhesion to engineered surfaces." *Colloids and Surfaces B: Biointerfaces* **2008**, 62, 232-237.

Maronek, A. E. "Evaluating acceptability of potable water tank coatings." *Journal of Protective Coatings and Linings* **1988**, 5 (7), 40-45.

Maurice, P. "Applications of atomic-force microscopy in environmental colloid and surface chemistry." *Colloids and Surfaces A: Physicochemical and Engineering Aspects* **1996**, 107, 57-75.

Meinders, J. M.; van der Mei, H. C.; and Busscher, H. J. "Deposition efficiency and reversibility of bacterial adhesion under flow." *Journal of Colloid and Interface Science* **1995**, 176, 329-341.

Méndez-Vilas, A.; Gallardo-Moreno, A. M.; González-Martín, M. L.; Calzado-Montero, R.; Nuevo, M. J.; Bruque, J. M.; and Pérez-Giraldo, C. "Surface characterisation of two strains of *Staphylococcus epidermis* with different slime-production by AFM." *Applied Surface Science* **2004**, 238, 18-23.

Millsap, K. W.; Reid, G.; van der Mei, H. C.; Busscher, H. J. "Adhesion of *Lactobacillus* species in urine and phosphate buffer to silicone rubber and glass under flow." *Biomaterials* **1996**, 18, 87-91.

Montanaro, L.; Campoccia, D.; Rizzi, S.; Donati, M. E.; Breschi, L.; Prati, C.; and Arciola, C. R. "Evaluation of bacterial adhesion of *Streptococcus mutans* on dental restorative materials." *Biomaterials* **2004**, 25, 4457-4463.

Murphy, E. M.; Zachara, J. M.; and Smith, S. C. "Influence of Mineral-Bound Humic Substances on the Sorption of Hydrophobic Organic Compounds." *Environmental Science and Technology* **1990**, 24, 1507-1516.

Murphy, E. M.; Zachara, J. M.; Smith, S. C.; and Phillips, J. L. "The sorption of humic acids to mineral surfaces and their role in contaminant binding." *The Science of the Total Environment* **1992**, 117/118, 413-423.

Murphy, E. M.; Zachara, J. M.; Smith, S. C.; Phillips, J. L.; and Wietsma, T. W. "Interaction of Hydrophobic Organic Compounds with Mineral-Bound Humic Substances." *Environmental Science and Technology* **1994**, 28, 1291-1299.

Namguk, H.; Amy, G.; Plottu-Pecheux, A.; and Yoon, Y. "Identification of nanofiltration membrane foulants." *Water Research* **2007**, 41, 3936-3947.

Parikh, S. J. and Chorover, J. "ATR-FTIR spectroscopy reveals bond formation during bacterial adhesion to iron oxide." *Langmuir* **2006**, 22 (20), 8492-8500.

Park, S.-J. and Kim, S.-B. "Adhesion of *Escherichia coli* to iron-coated sand in the presence of humic acid: a column experiment." *Water Environment Research* **2009**, 81 (2), 125-130.

Rijnaarts, H. H. M.; Norde, W.; Lyklema, J.; and Zehnder, A. J. B. "DLVO and steric contributions to bacterial deposition in media of different ionic strengths." *Colloids and Surfaces B: Biointerfaces* **1999**, 14 (1-4), 179-195.

Ryan, J. N.; Elimelech, M.; Ard, R. A.; Harvey, R. W.; and Johnson, P. R. "Bacteriophage PRD1 and silica colloid transport and recovery in an iron oxide-coated sand aquifer." *Environmental Science & Technology* **1999**, 33, 63-73.

Sader, J. E.; Larson, I.; Mulvaney, P.; and White, L. R. "Method for the calibration of atomic force microscope cantilevers." *Review of Scientific Instruments* **1995**, 66 (7), 3789-3798.

Salerno, M. B.; Logan, B. E.; and Velegol, D. "Importance of molecular details in predicting bacterial adhesion to hydrophobic surfaces." *Langmuir* **2004**, 20 (24), 10625-10629.

Sanin, S. "Effect of surface properties and flow regime on the transport of bacteria in groundwater: An experimental approach." *Turkish Journal of Engineering and Environmental Sciences* **2004**, 28 (5), 317-324.

Schmalz, G. "Uber Glätte und Ebenheit als Physikalisches und Physiologishes Problem." *Zeitschrift des Vereines deutscher Ingenieure* **1929**, 1461-1467.

Senden, T. J. and Ducker, W. A. "Experimental determination of spring constants in atomic force microscopy." *Langmuir* **1994**, 10 (4), 1003-1004.

Serry, F. M. "Improving the accuracy of AFM force measurements: The thermal tune solution to the cantilever spring constant problem." Veeco Instruments **2005.**

Shellenberger, K. and Logan, B. E. "Effect of molecular scale roughness of glass beads on colloidal and bacterial deposition." *Environmental Science & Technology* **2002**, 36, 184-189.

Smets, B. F.; Grasso, D.; Engwall, M. A.; and Machinist, B. J. "Surface physiochemical properties of *Pseudomonas fluorescens* and impact on adhesion and transport through porous media." *Colloids and Surfaces B: Biointerfaces* **1999**, 14 (1-4), 121-139.

Stefano, F. S.; Bosma, T. N. P.; Harms, H.; and Zehnder, A. J. B. "Bivalent cations increase both the subpopulation of adhering bacteria and their adhesion efficiency in sand columns." *Environmental Science and Technology* **2000**, 34 (6), 1011-1017.

Switalski, L. M. and Butcher, W. G. "An *in vitro* model for adhesion of bacteria to human tooth root surfaces." *Archives of Oral Biology* **1994**, 39 (2), 155-161.

Tobin, J. O.; Swan, R. A.; and Bartlett, C. L. "Isolation of *Legionella pneumophila* from water systems: methods and preliminary results." *British Medical Journal* **1981**, 282, 515-517.

Truesdail, S. E.; Lukasik, J.; Farrah, S. R.; Shah, D. O.; and Dickinson, R. B. "Analysis of bacterial deposition on metal (hydr)oxide-coated sand filter media." *Journal of Colloid and Interface Science* **1998**, 203 (2), 369-378.

Vadillo-Rodríguez, V. *Macroscopic and microscopic approaches towards bacterial adhesion*. Stichting Drukkerij de Regenboog, Groningen, The Netherlands, 2004.

Vadillo-Rodríguez, V. and Logan, B. E. "Localized attraction correlates with bacterial adhesion to glass and metal oxide substrata." *Environmental Science & Technology* **2006**, 40, 2983-2988.

Veeco Instruments. *Multimode SPM Instruction Manual*. Santa Barbara: Veeco Instruments, 2004.

Walker, J. T., Dowsett, A. B., Dennis, P. J. L, and Keevil, C. W. "Continuous culture studies of biofilm associated with copper corrosion." *International Biodeterioration* **1991**, 27, 121-134.

Walker, S. L. "Influence of bacterial surface polymers on bacterial adhesion and transport in groundwater environments." *Journal of Harbin Institute of Technology* **2005**, 12, 19-26.

Whitehead, K. A.; Rogers, D.; Colligon, J.; Wright, C.; and Verran, J. "Use of the atomic force microscope to determine the effect of substratum surface topography on the ease of bacterial removal." *Colloids and Surfaces B: Biointerfaces* **2006**, 51, 44-53.

Xu, L.-C., Vadillo-Rodríguez, V., and Logan, B. E. "Residence time, loading force, pH, and ionic strength affect adhesion forces between colloids and biopolymer-coated surfaces." *Langmuir* **2005**, 21, 7491-7500.

Yang, K.; Lin, D.; and Xing, B. "Interactions of Humic Acid with Nanosized Inorganic Oxides." *Langmuir* **2009**, 25, 3571-3576.

Young, R. J., Ward, F. S. "The Topografiner: An Instrument for Measuring Surface Microtopography." *Review of Scientific Instruments* **1972**, 43 (7), 999.

Zita, A. and Hermansson, M. "Effects of Ionic Strength on Bacterial Adhesion and Stability of Flocs in a Wastewater Activated Sludge System." *Applied and Environmental Microbiology* **1994**, 60 (9), 3041-3048.